QUARTERLY STATUS REPORT NO. 11

Period 23 March 1967 - 22 June 1967

DESIGN, DEVELOPMENT, FABRICATION AND INSTALLATION OF 105-INCH LUNAR AND PLANETARY TELESCOPE AT McDONALD OBSERVATORY

Contract NASr-242
SC/44-012-025-(056)

Project Director: Harlan J. Smith
Director, McDonald Observatory

Department of Astronomy, The University of Texas
Austin, Texas

QUARTERLY STATUS REPORT No. 11

Period 23 March 1967 - 22 June 1967

DESIGN, DEVELOPMENT, FABRICATION AND INSTALLATION OF 105-INCH LUNAR AND PLANETARY TELESCOPE AT McDONALD OBSERVATORY

Contract NASr-242

A. Outline of Progress Prior to this Reporting Period

The telescope design has been completed, along with the technical concept and basic mechanical and optical requirements of a horizontal coude spectrograph; work is well under way on all major components. In particular, Davidson Optronics has started figuring the primary mirror and the f/9, f/33, and f/18 secondaries, also the first and second coude flats. Davidson is figuring the short coude camera (both collimator and camera mirrors), while the optical shop of the Arizona Lunar and Planetary Laboratory is figuring the medium camera. Along with many smaller parts, Westinghouse has completed the polar axis shaft to the point of being ready to stress-relieve before beginning to machine the hydraulic bearings, and the housing for the large declination axis ball bearings has been fabricated.

B. Progress during the Period 23 March 1967 - 22 June 1967

1. Mechanical

All major manufacturing holds on the mechanical construction were broken by an agreement on the control system concept at a meeting with Westinghouse May 22, 1967. Westinghouse produced a mechanical drawing layout for the telescope drive ~~that~~ was aeceptable to Texas. The necessary brackets for the control system have been welded to the two major parts, polar axis and declination housing, and these two parts have been stress relieved and are started on the machining cycle.

2. Controls

After difficulties referred to in previous Reports and in Section 3 of this Report, Westignhouse produced on May 22 a control concept that was accepted by Texas, and all work on other variations was canceled. Figures 1 and 2 show the system in block diagram

form A

form. A single permanent magnet D. C. Motor is used for both slew and track. The shaft for the drive motor and worm gear is one piece with no couplings or clutches. Backlash is removed from the worm by preloading the worm against the worm wheel with a separate permanent magnet D. C. torque motor coupled to the worm wheel through a spur gear. Power is applied to the drive motor by a linear D. C. amplifier (stabilized by a current feedback loop) for track, set, and guide modes and through a high-power silicon-controlled rectifier amplifier for the slew modes. The preload motor receives its commands through a simple logic circuit that applies power in the necessary fine increments to keep the worm and worm wheel from separating.

The control logic ~~for the telescope drive~~ is basically a straightforward pulse counting system. A precision frequency from a crystal-controlled oscillator is divided down to furnish 300 pulses per second to correspond to earth's rotational rate of 15 arc seconds per second. This signal is compared with the feedback frequency from a high resolution digital tachometer (1 pulse for each .05 arc seconds of telescope movement) rigidly connected to the drive motor and any difference between the track command frequency and the tachometer feedback frequency is converted to an analog voltage and applied to the drive motor to change the track rate of the telescope.

Three additional input frequencies can be selectively added to or substracted from the basic tracking rate frequency to make fine adjustments to the track rate, obtain a "set rate" for coarse adjustments, and obtain a "guide rate" to compensate for varying seeing condirions.

Computer simulation studies of the drive system using the selected motor sizes, compensation networks, amplifier gains and the calculated telescope inertia and bearing friction lead to expectation of a control limit cycle oscillation with a magnitude corresponding to one or two pulses of the tachometer; this would give a steady-state rotational accuracy of the worm shaft of 0.1 arc second (referred to the optical axis of the telescope).

3. Westinghouse Contract

The problems with Westinghouse concerning target cost have not been resolved during this reporting period. Westinghouse declined to accept the NASA suggestion that any increase in fee for Critical Path Planning be incentive fee based on delivery time.

Texas reported the contract problems at NASA Headquarters on April 26, 1967. At this meeting, Texas suggested the possibility of selective

D

cancellation of parts of the Westinghouse contract in order to break the deadlock. In particular, at this time Texas considered Westinghouse performance on the control design and manufacture so slow and uncertain as to warrant cancellation, although performance on the large fabricated metal parts indicated that Westinghouse could finish these. NASA suggested that Texas look for a possible alternate company to complete the whole mechanical mount and control system. NASA also asked for a review of the project by The University administration.

In preparation for possible cancellation, Texas requested Westinghouse to prepare a review for The University administration covering:

a. Physical inventory of parts, drawings and reports completed.

b. Detailed plan to complete the contract.

c. Specific suggestions as to how completion can be assured no later than July 1968.

The review was held at Westinghouse May 26, 1967. Texas was represented by:

Mr. Jack Josey, Vice Chairman, Board of Regents
Dr. Norman Hackerman, Vice Chancellor for Academic Affairs
Mr. E. D. Walker, Vice Chancellor for Business Affairs
Dr. George Kozmetsky, Executive Associate for Economic Affairs
Mr. James Colvin, Business Manager, Main University
Mr. Burnell Waldrep, University Attorney
Dr. Harlan J. Smith, Director McDonald Observatory
Mr. Charles E. Jenkins, Project Manager
Mr. Don Bresie, Project Engineer

The results of the meeting were reported at NASA Headquarters, June 7, 1967, the salient points being:

a. Considering the facts presented in the above review including Westinghouse provision of a satisfactory control system, and the negative results from a Texas survey of alternate companies, Texas prefers to continue with Westinghouse.

b. Through the office of Mr. Walker and Dr. Kozmetsky, The University administration will give additional support to the Project Director.

c. Texas and NASA will hold monthly review meetings to evaluate progress.

4. Optics

Davidson Optronics continued to make good progress on the optics. H. Smith, R. Tull, and D. Bresie visited Davidson on June 22, 1967, to review the work. Davidson has solved the problem of supporting the large and relatively thin 105-inch primary mirror for in-process testing, by using a mercury bag of ingenious design. The primary has now been ground to a point between a sphere and a parabola, and Davidson has encountered no problems in working the quartz. A preliminary test was made by supporting the partially completed mirror on two edge supports, with ambiguous results concerning the presence of appreciable support deformations. The final figure is necessary before such a test can be sensitive enough to demonstrate the presence or absence of deformations detectable in telescope use.

5. Coude Spectrograph

The concept drawings for the mechanical parts of the coude spectrograph have been completed and accepted. C. W. Jones is now in the process of completing the details for bid drawings and writing a specification. These are scheduled to be completed by August and bids for the manufacture received in September.

The spectrograph frame has been installed in the dome by the construction contractor. The design of the kinematic supports for the frame has been completed and bids for their manufacture have been solicited. No problems are anticipated with the frame or the supports.

The major optical elements have been purchased and figuring is nearing completion on both the 40-inch and 59-inch coude camera blanks and their companion collimators. An acceptance test for the 40-inch is scheduled at Davidson Optronics in August, and a progress review meeting at the University of Arizona on the 59-inch is also scheduled in August.

6. Dome and Building

Although not financed by this contract, the construction of the piers and the rotating dome and building necessary to support the dome constitutes a parallel project, obviously integral to the schedule of the telescope erection and installation of the coude spectrograph.

The C. H. Leavell Company of El Paso, Texas has essentially completed the steel framing for the building and is now installing the prefabricated dome. The relatively minor problems which have arisen with the dome seem to be solved, and completion is expected about January 1968. Figure 3 shows the dome construction as of mid-June.

As a note of extra interest, a construction contract has been awarded for the planned Transient Quarters (16 sleeping rooms, dining area,

conference area, and housekeeper quarters) and completion is scheduled for the first of January 1968.

C. Financial Report

NASA Form 1030 (2-64) for this contract is submitted quarterly by the Auditor's Office of The University of Texas.

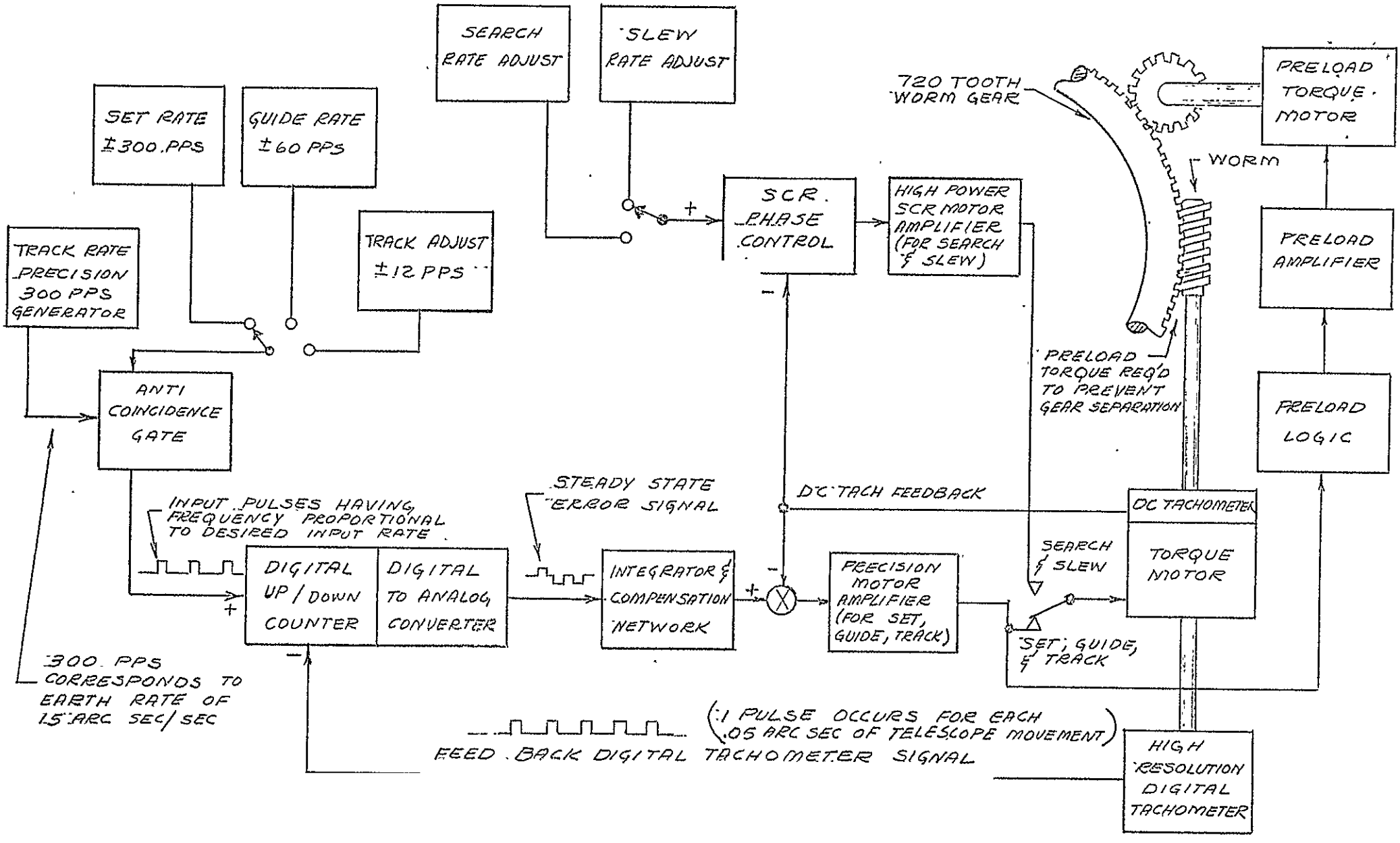

POLAR AXIS DRIVE CONTROL SYSTEM

Figure 1

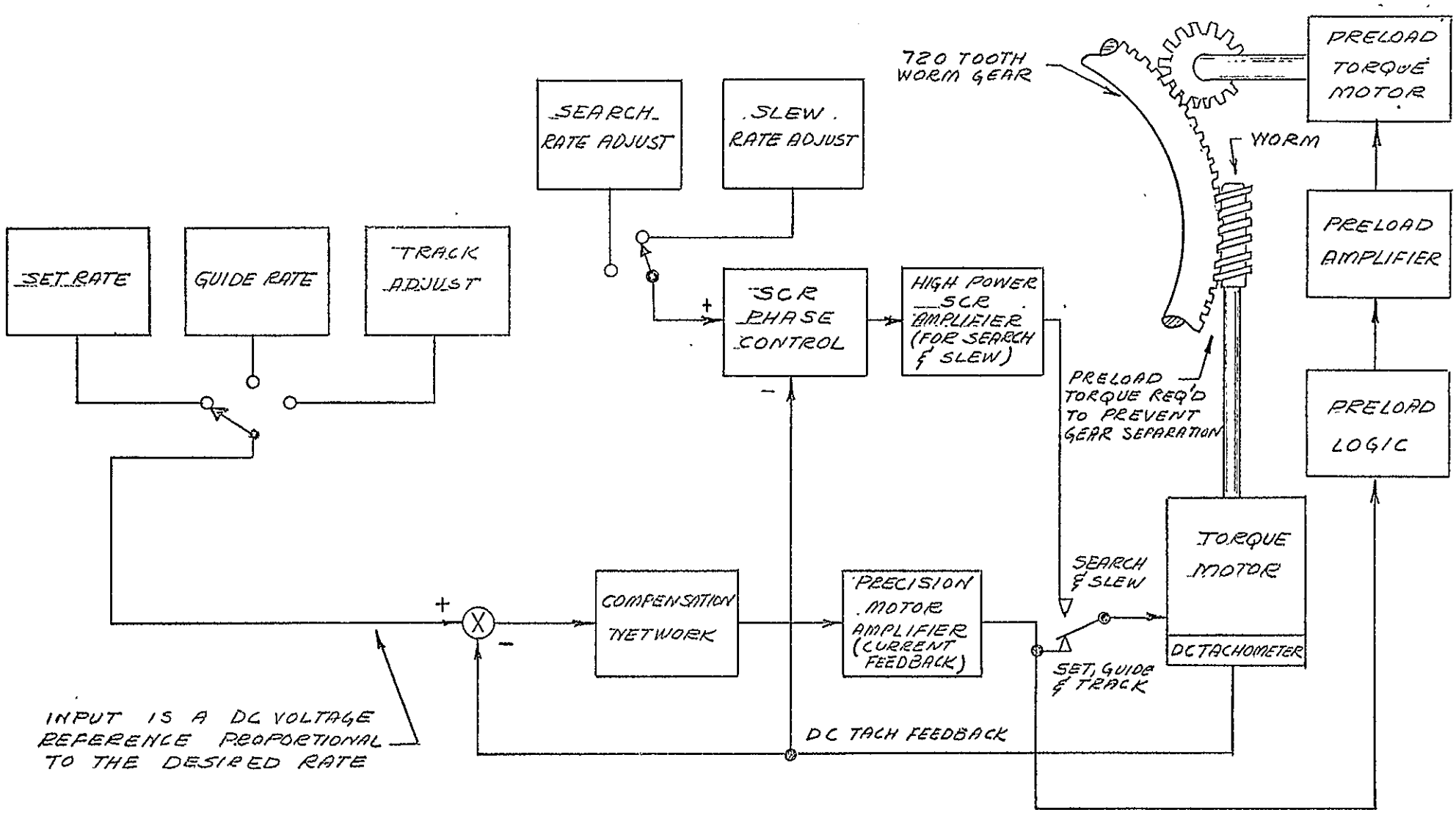

DECLINATION AXIS DRIVE CONTROL SYSTEM

Figure 2

NOT REPRODUCIBLE

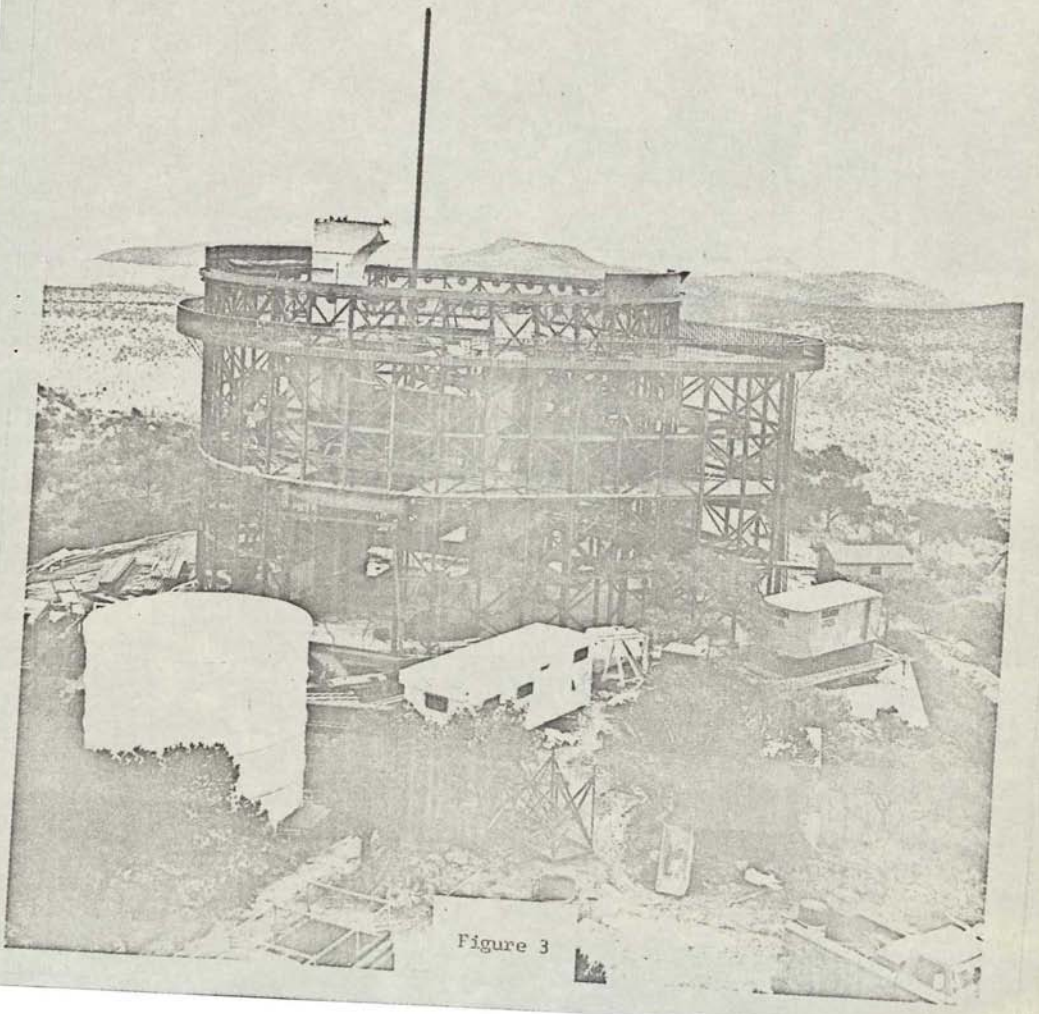

Figure 3

1. Hydrogen Bubble Generator

Generation of hydrogen bubbles within a stream as a means of flow visualization is widely used for fluid dynamic studies. The technique is fully described in the literature (Ref. 1). It consists, simply, of generating hydrogen bubbles by electrolysis of water in the vicinity of the region of flow under study. If a pulsating electric current is employed, the generation of bubbles will be periodic. Under these conditions, a still photograph of two or more rows of bubbles permits the estimation of fluid velocity along the line of the wire electrode when the electrical pulsation rate is known.

A monopolarity pulse generator was designed and constructed for this purpose. (See the circuit diagram in Figure II-5 and the photo in Figure II-6.) Timing is obtained by counting down from the 60 Hz power mains. The pulse generator is capable of providing an adjustable voltage dc pulse (15 to 150 volts) at either 7.5, 3.8, 1.9, or 0.94 pulses per second. The duration of each pulse can be adjusted to last from approximately five percent to 50 percent of the pulsing period. This design is sufficiently flexible that higher or lower pulse rates could be obtained, if necessary, by simple circuit modifications. Operation of this generator was quite satisfactory; however, some difficulties existed initially with the wire electrode. Uniformity of the bubbles was improved by electroplating with platinum (Ref. 2).

One problem that must be taken into account when bubbles are used for flow visualization is the effect of buoyancy. A vertical velocity component always exists. Since the buoyant force is proportional to bubble volume (radius^3) and the viscous drag force is proportional to velocity times radius (Stokes' Law), the rate of rise of the bubbles should be proportional to the square of the bubble radius. Thus, generation of small bubbles minimizes the buoyancy effect. The pulse generator should be operated at conditions that give the smallest uniform bubbles. Performance of the bubble generator in a test tank is shown in Figure II-7. For this photo a five mil wire was used; the voltage was 130 volts; the repetition rate was 3.8 pulses per second; and the pulse duration was approximately 0.014 second. These settings appeared to yield the smallest, relatively uniform bubbles distributed fairly evenly over the wire. As can be seen from the scale, the separation between wave fronts is approximately two millimeters. At the pulse rate of 3.8 pulses per second, this corresponds to a velocity of rise of 7.52 millimeters per second. Measurements from the original print of Figure II-7 show the increase in velocity of the bubbles as they rise from the wire to reach their limiting velocity in about 4.5 millimeters of rise. Considerable definition has been lost in the reproduction process used for this document.

Figure II-8 shows a typical bubble flow pattern in the scaled-up model test fixture. Once again, considerable definition has been lost in the reproduction process used for this document and an artists' rendering of the flow pattern is shown below the print of the photograph. Note the way that the bubble fronts are piling up at the edge of the left channel and the irregularities in the other channels. This is indicative of ripples in

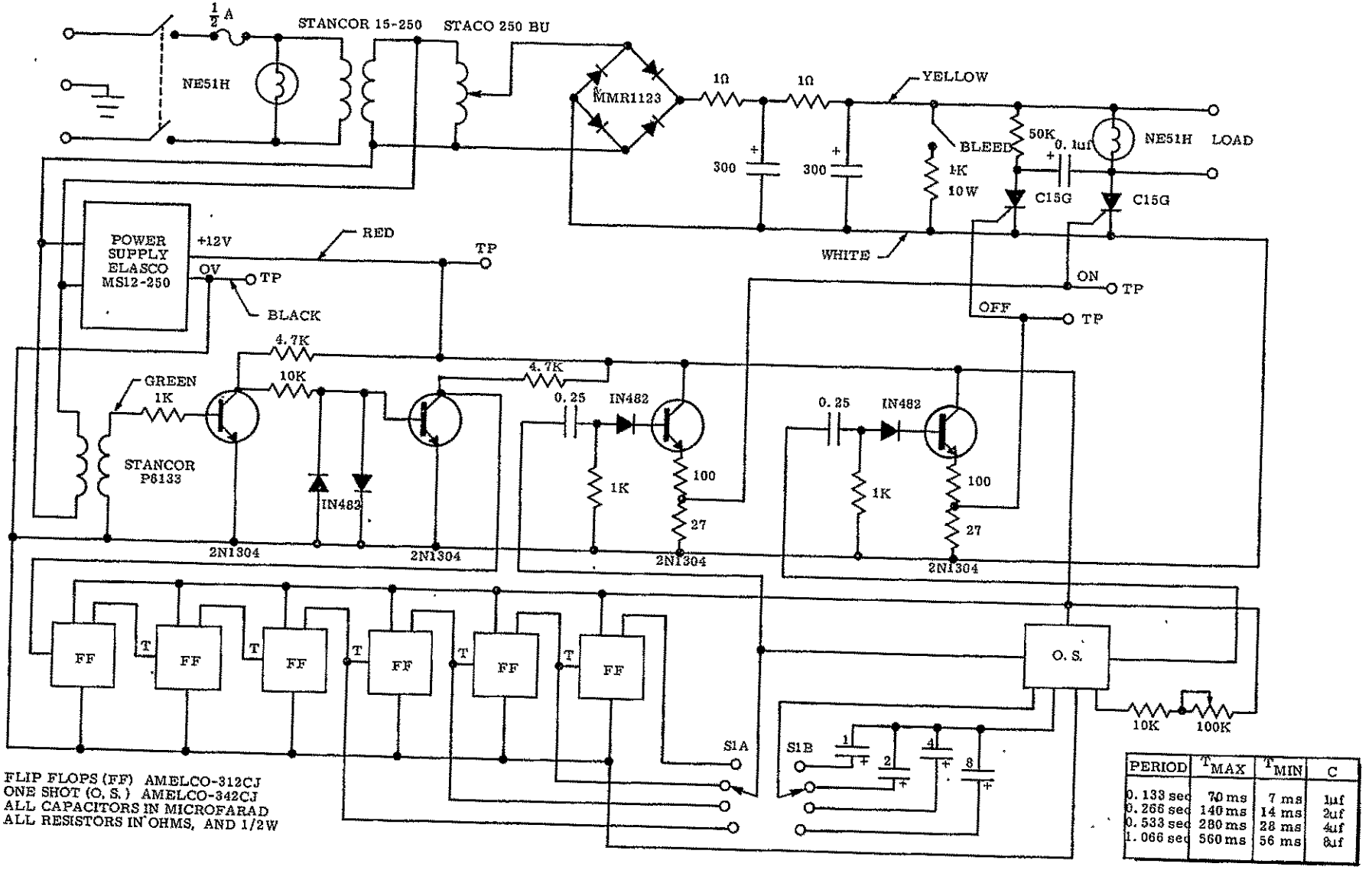

PERIOD	T_{MAX}	T_{MIN}	C
0.133 sec	70 ms	7 ms	1uf
0.266 sec	140 ms	14 ms	2uf
0.533 sec	280 ms	28 ms	4uf
1.066 sec	560 ms	56 ms	8uf

Figure II-5. Schematic of the Pulse Generator

Figure II-6. External View of the Pulse Generator

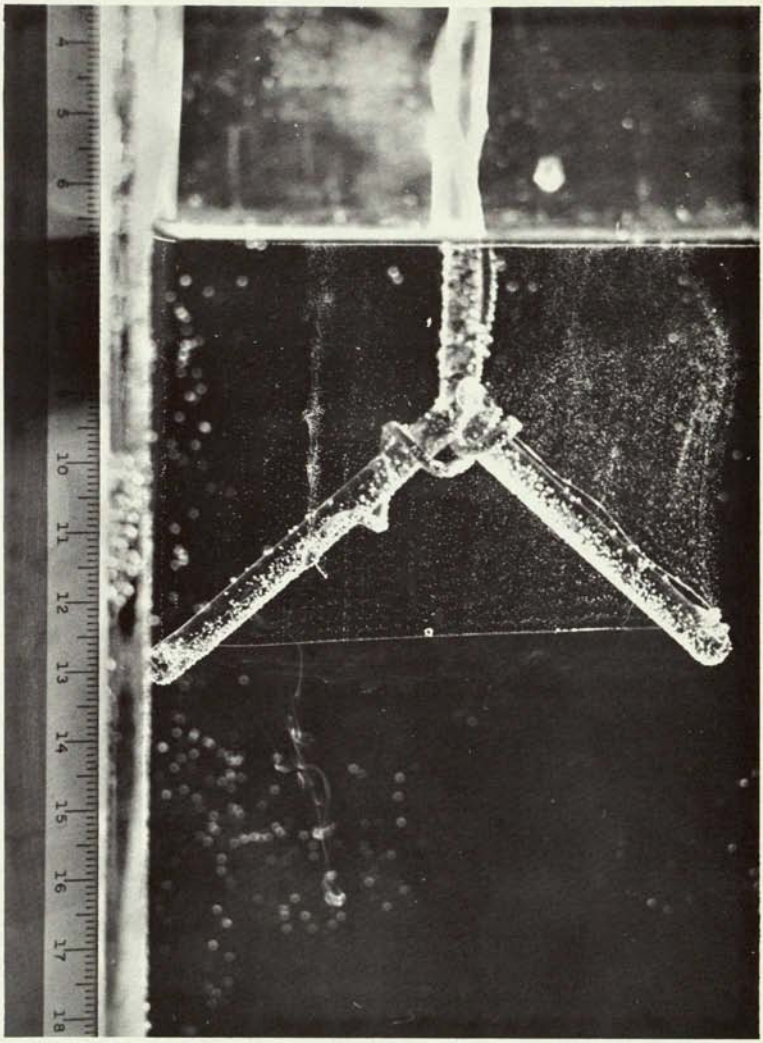

Figure II-7. Hydrogen Bubbles Rising Due to Buoyancy

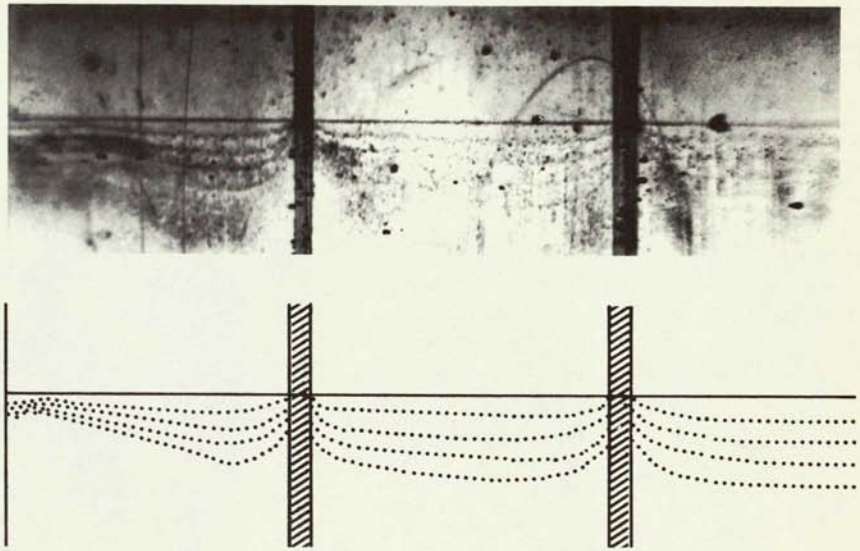

Figure II-8. Bubble Pattern Visualization of Flow in the Test Channel

the membrane. The slope of these profiles was used as a check on the positioning accuracy of the membrane and as a means of measuring the amount of channeling which was occurring.

2. Conductivity Probe for Salt Concentration Measurements

a. Probe Design. The conductivity probe consisted of a long, tapered glass capillary tube containing a one mil diameter platinum wire. The wire was exposed at the pointed tip where the glass insulation had tapered to zero. Since such probes were not known to be available commercially, the fabrication technique was developed for this study. With our technique, after a little practice, probes could be made easily by hand starting with six millimeter pyrex tubing and one mil platinum wire. As is shown below, these probes are quite uniform in their electrical characteristics. The major problem associated with using these probes was their inherent fragility. Care must be taken at all times in the installation and mechanical operation of these probes. When care was used in handling, the probes were found to operate uniformly and reliably.

The fragility of the probes was the result of their very small diameter. A small diameter was needed for two reasons, one electrical and the other fluid dynamic. The effective region being observed by a spherical conductivity electrode is a spherical region approximately five diameters larger than the probe tip. The theoretical basis for this is given in Appendix B. The region of observation of the probe must be small compared to the channel dimensions (0.25 inch high) so that a reasonably accurate conductivity profile can be obtained, thus, a small diameter tip is necessary for useful electrical measurements.

Since the conductivity probe was used to obtain concentration profiles, the probe itself must not disturb the pre-existing profile in the act of measuring. If the probe presents too large an obstruction to flow, then effects occur upstream to the probe and change the concentration profile by inducing mixing. Thus, a small diameter tip and a streamlined taper was also necessary for fluid dynamic reasons.

This conductivity probe was used in conjunction with a commercially obtained 25 KHz bridge (Tektronix 3C66) which is a plug-in unit to our Tektronix 561A oscilloscope with a 3B4 time base plug-in unit.

A probe holder fixture was constructed for the main test fixture. This holder is shown in Figure II-9. The glass probe was fastened to a stainless steel tube by a shrink-fit sleeve and the device was made water-tight with Pliobond cement. A platinum disk located within the liquid near the exit end of the test apparatus was used as the indifferent electrode. The device was used to provide conductivity data from our main test fixture.

b. Probe Performance Tests. During the time when the main test fixture was being fabricated, tests were carried out on the electrical

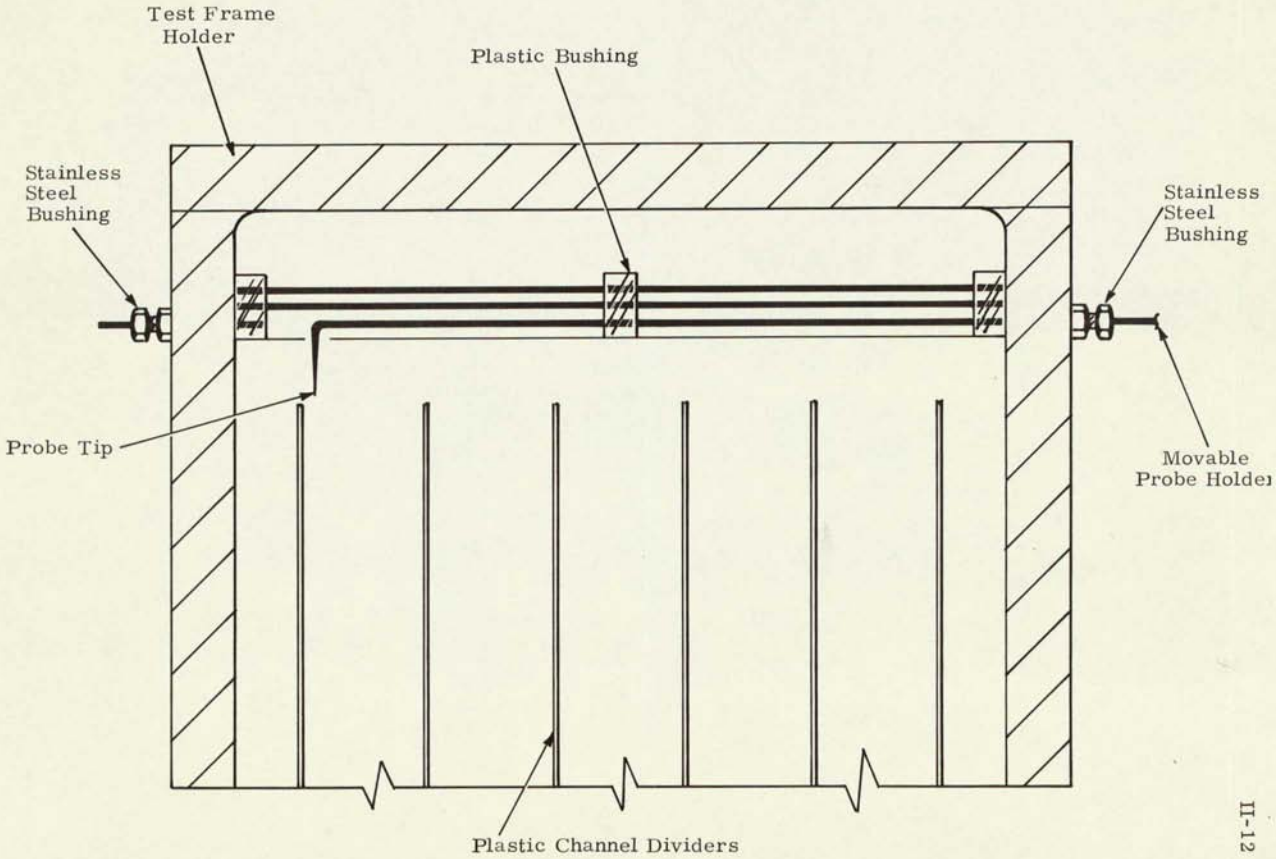

Figure II-9. Conductivity Probe Mounted in the Main Test Apparatus

performance characteristics of the conductivity probes. A number of probes were fabricated and tested in known solutions of reagent grade sodium chloride (NaCl) in distilled water. Table II-1 shows the aging characteristics of five identically constructed probes. It can be seen that there is a high degree of uniformity in characteristics and that they are quite stable after a "running-in" period.

An experiment was performed to determine the region of observation of our conductivity probes. This consisted of introducing a low velocity jet stream into a tank of water. The conductivity of the jet stream was chosen to be considerably higher than that of the water in the tank. The conductivity probe was then inserted into the tank and conductivity was measured continuously as the probe passed into the stream. The water in the jet was dyed slightly for flow visualization. The experimental set-up is shown in Figure II-10. It was found that there was no apparent mixing between the jet stream and the tank water and that the probe was able to measure the location of the boundary to the accuracy of the advance mechanism. The advance mechanism was a converted microscope stage with a vernier scale to one-tenth millimeter (or 0.004 inch).

TABLE II-1. AGING DATA ON CONDUCTIVITY PROBES

Probe No.	Storage Conditions	Oscilloscope Deflection in Arbitrary Units* Days 0	2	5	6	7	9	13	14	21
1	distilled H_2O	16	14	11	11	12	11	9	11	10
2	air	10	10	11	10	11	10	9	10	11
3	air	10	11	13	13	14	11	11	12	11
4	100 ppm saline	10	11	11	11	12	9	9	12	11
5	air	14	This probe tested only on initial fabrication and at termination of the test							11

*The arbitrary units are based on using the same bridge settings as are used in all calibration runs with known solutions.

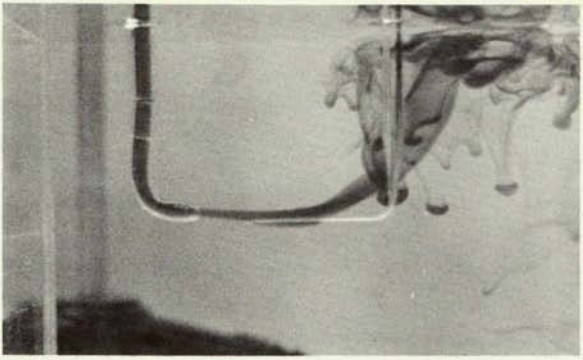

a. Conductivity Probe at the Lower Edge of a Jet Stream

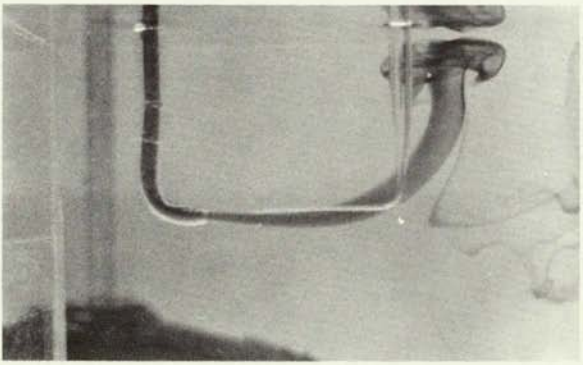

b. Conductivity Probe at the Upper Edge of a Jet Stream

Figure II-10. Experimental Set-Up to Test Position Sensitivity of the Conductivity Probe

The conductivity probe was calibrated periodically and the calibration was checked prior to each test run carried out in the test apparatus. The probes were found to be quite linear over a wide range of concentration values. In these tests, chloride ion concentrations were determined with a standard water test procedure using 0.0141N mercuric nitrate as the titrating reagent and phenylcarbazone as the end-point indicator. A typical calibration curve is shown in Figure II-11.

3. Cellophane Testing

The uniformity of the dialyzing membrane is an extremely important parameter. It is apparent that if the membrane used during one test has significantly different diffusion characteristics from that used in a following test, the results of secondary flow would be masked by the variation in membrane permeability. Also, if the membrane permeability varies greatly from area to area within one test section it would be impossible to have confidence in concentration profile data.

For these reasons tests were carried out to establish whether the uniformity of cellophane is sufficient to permit us to use it as the dialyzing membrane in the main test fixture. Cellophane was obtained from DuPont Corporation (215PD-62 uncoated cellophane). Five samples were selected from widely separated locations on our first lot of cellophane and were tested in an elementary diffusion test apparatus. The test fixture is shown in Figure II-12. Agitation was used on both sides of the membrane section under test. In this test, urea tagged with carbon-14 was used as the solute. Samples were taken from the low concentration bath in the beaker at the end of one and two hours and counted for radioactivity level. The sample mean after one hour was 24,140 counts per minute and the sample variance was 2,450. After two hours the sample mean and variance were 37,748 and 4,440 counts per minute, respectively. It is felt that since the variance is about 10 percent of the mean the cellophane is sufficiently uniform to permit us to use it in the initial tests in our scaled-up model dialyzer. Since relatively large membrane areas are used in our test apparatus, the 10 percent variation over small areas will tend to be averaged out.

Each sample of cellophane was tested under identical conditions in our simple test apparatus. Therefore, uniformity of the cellophane could be evaluated in this device. It is questionable whether this test apparatus is adequate for absolute measurement of membrane permeability. Although an absolute measure of membrane permeability is not of primary importance for the performance of our study, it is interesting to note the values for diffusion constant obtained for our sample of cellophane. Over the first hour, the mean value for diffusion constant (for urea) was 0.167×10^{-5} square centimeters per second and the mean value was 0.172×10^{-5} square centimeters per second over the second hour interval. These values fall within the range of diffusion constants of cellophane for NaCl as recently reported by Smith, et al. (Ref. 3). Meltzer, et al. (Ref. 4) showed that for the cuprophane type of cellophane dialysis times were approximately equal for NaCl solutions and urea solutions. Meltzer defined dialysis time as the time required to change the difference in concentration for 0.1 M to 0.01 M in his test apparatus.

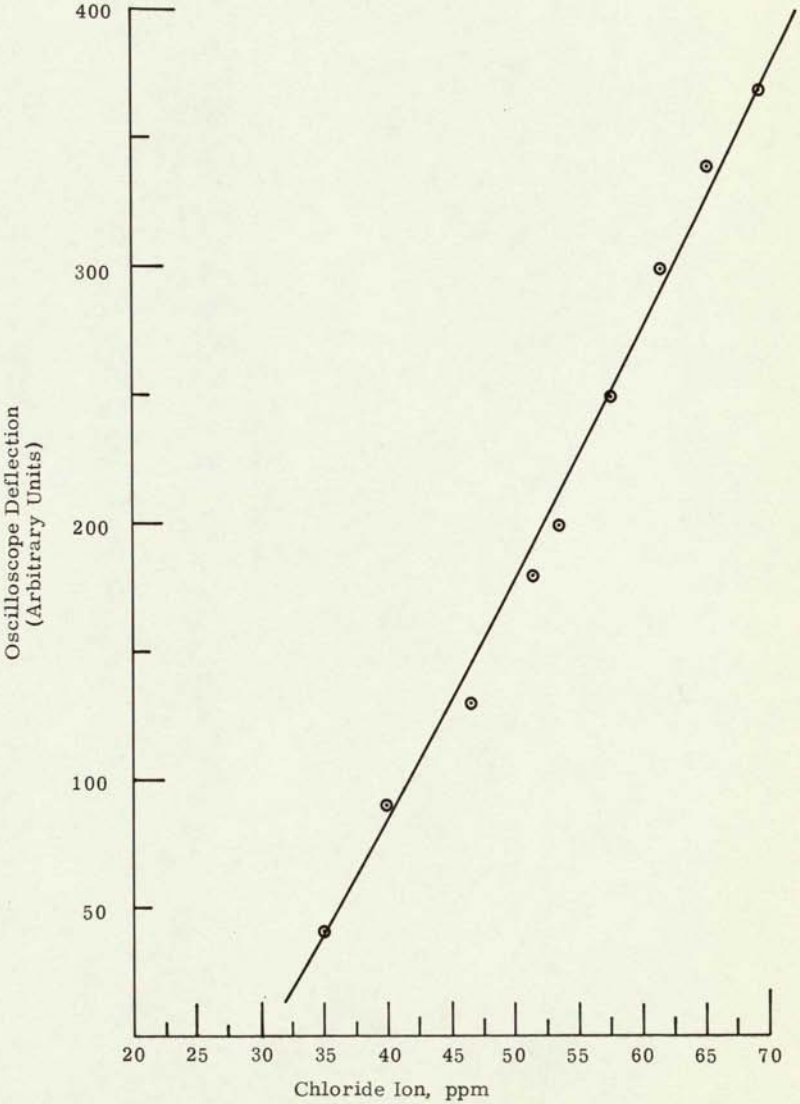

Figure II-11. A Typical Calibration Curve of the Conductivity Probe Obtained with the Main Test Apparatus

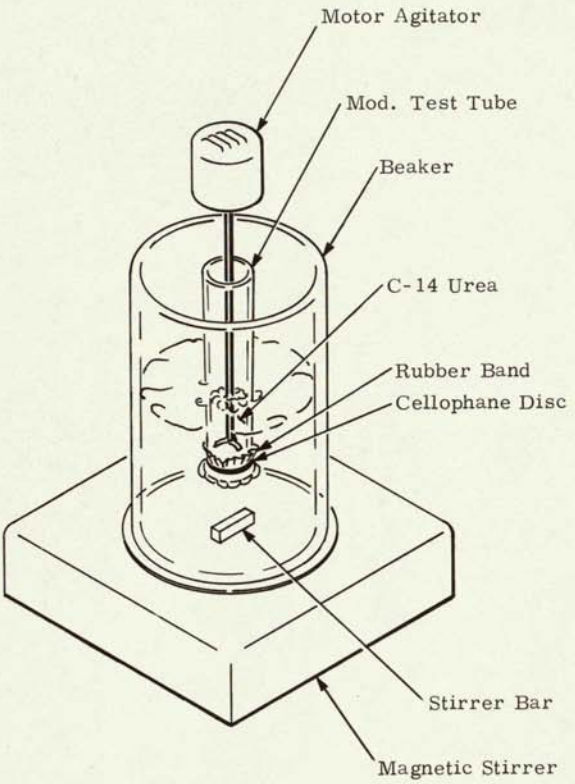

Figure II-12. Test Apparatus for the Measurement of Membrane Permeability

C. Experimental Procedures

The experimental plan of the investigation was to construct the scaled-up model and to measure concentration and velocity patterns for unperturbed and geometrically perturbed flow conditions. The unperturbed flow case served as a baseline comparable to a conventional Kiil dialyzer against which performance of perturbed flow cases could be compared. While the large test apparatus was being assembled and tested for the baseline case of parallel channels, some exploratory experiments were carried out in a simple test apparatus to examine the effects of various geometrical perturbers on flow.

1. Exploratory Flow Perturbation Experiments

A small test apparatus was constructed for the purpose of gaining insight into the types of flow perturbations obtained with various geometric structures under the low Reynolds number conditions of hemodialyzers. This apparatus consisted of a transparent trough which could be tilted to cause flow from an upstream weir through channels with various selected test geometric shapes to a downstream weir. Liquid was collected at the downstream end and recirculated by means of a pump. A standpipe and bypass line upstream of the first weir were used to maintain a constant pressure feed. Figure II-13 is a photo of the small test fixture.

This apparatus was used for flow visualization of the pattern of stream lines by dye injection as the liquid flowed through the test channels. In this way, it was possible to perform an initial screening of candidate flow perturbation concepts. Our initial experiments with this apparatus were directed at generating longitudinal vorticity in order to cause intensive enough secondary flow to move fluid from the boundary into the interior of the channel. A single dyed stream line will appear as a helix as it progresses down the channel when longitudinal vorticity is introduced. Such a flow pattern contains a significant velocity component transverse to the main flow and, by continuity, normal to the channel walls for transport of solute and does not necessarily introduce excessive pressure drop along the length of the channel.

Diffusion across a membrane was not included in this small test fixture and no measurements of concentration or velocity profiles were made. Average velocity and channel dimensions were measured.

With Reynolds numbers that were appropriate for dialyzers, no sustained longitudinal vortices were generated with our initial test perturbation geometries. It is believed that the velocities were so low that inertial effects were minimal. However, it was observed that in localized areas dyed stream lines could be made to cross and to flow from one boundary to the other thereby introducing the type of favorable secondary motion that was desired.

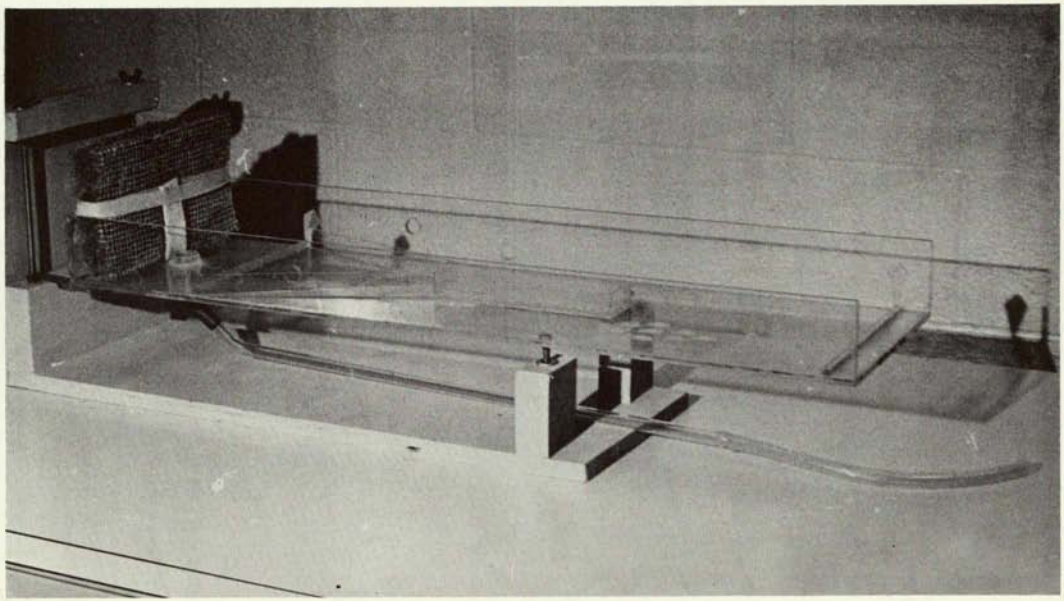

Figure II-13. Small Test Apparatus for Flow Visualization Studies

In this small test apparatus, geometries were used that were meaningful when translated into a membrane dialyzer. Therefore, types of patterns were used similar to those that could conceivably result from a membrane being draped over membrane support structures. Some examples of these are pyramidal shapes such as could occur using cone support structures as are used in some experimental artificial kidney dialyzers (Refs. 5 and 6) and ridged patterns that could result from long membrane supports set at some angle to the main direction of flow. Examples of test geometries that were tried are shown in Figures II-14 and II-15.

Photographs of dyed stream lines shown in Figure II-16 display the motion of stream lines forth and back between channel boundaries and the crossing of two stream lines as one rises from the lower to the upper boundary while the other drops from the upper to the lower boundary. The two dye streams were injected one above the other at the entrance to the test section. A two syringe infusion pump was used to inject a red and a green dye stream through hypodermic needles which were hand held in the appropriate position to display this effect.

2. Experiments in the Scaled-Up Dialyzer Model

The first set of data obtained in the test apparatus was a calibration of the conductivity probe. By using known concentration solutions in the supply reservoirs it was possible to calibrate the conductivity probe in terms of concentration. Convenient settings of the conductivity bridge were selected and fixed for the calibration run and all subsequent runs. As is shown in Figure II-11, the probe response was quite linear.

Following calibration of the probe, runs were made at various flow velocities. These runs were made in unperturbed parallel channels equivalent to a Kiil-type of structure. For these tests, a 600 ppm solution of NaCl in water was employed in the lower set of channels of the test apparatus and tap water was used in the upper set of channels. Concentration profile measurements were made in the upper set of channels. These conditions were selected because the probe had been calibrated at relatively low concentrations of NaCl. As expected, the concentration of NaCl is highest at the membrane boundary and decreases as the probe is moved away from the boundary. Results from a typical run are shown in Figure II-17.

Figure II-18 shows reasonable repeatability was obtained for two nearly equal velocity runs. The change in boundary layer dimensions with flow velocity was clearly seen.

Upon completion of the baseline cases, the apparatus was disassembled and longitudinal vortex generators of the type shown before in Figure II-15 were installed on both sides of the membrane as supports. Figure II-19 is particularly interesting because it shows the effect of these generators on the concentration profile. The solid line is the average curve used in the subsequent normalizations. It is also the approximate curve of the half channel width. The dotted curves are profiles taken one-half inch on either side of the half channel width. This curve is at approximately the same

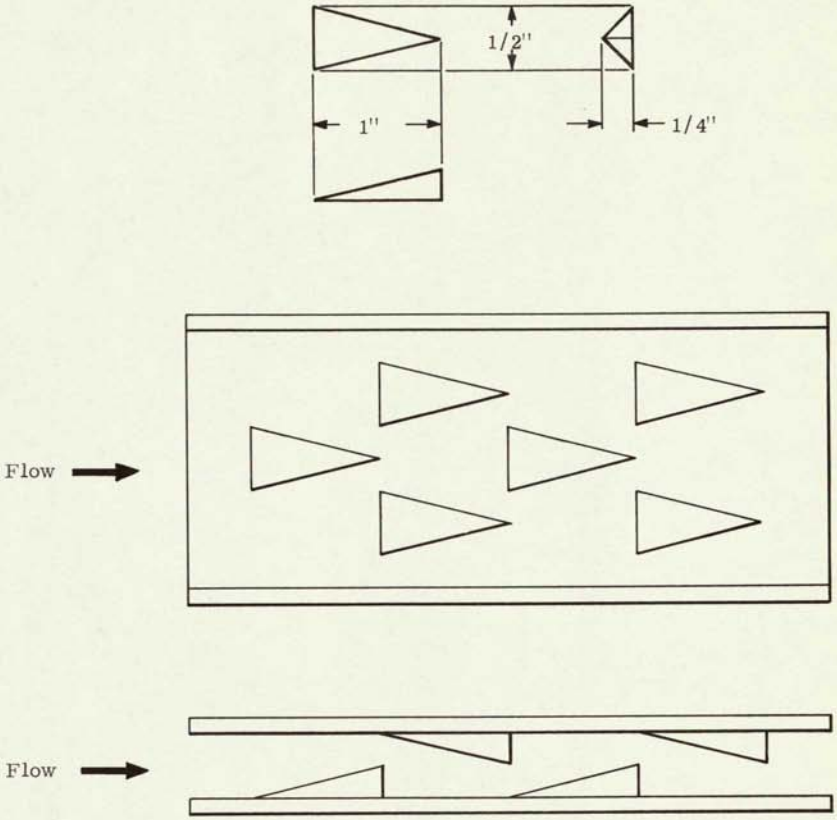

Figure II-14. An Example of One Type of Flow Perturbation Technique

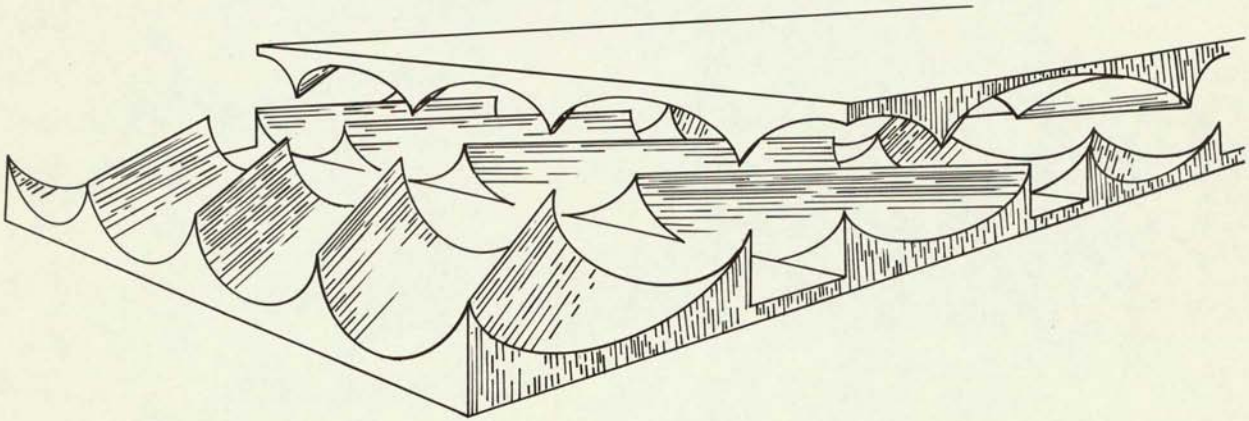

Figure II-15. An Example of Another Flow Perturbation Technique

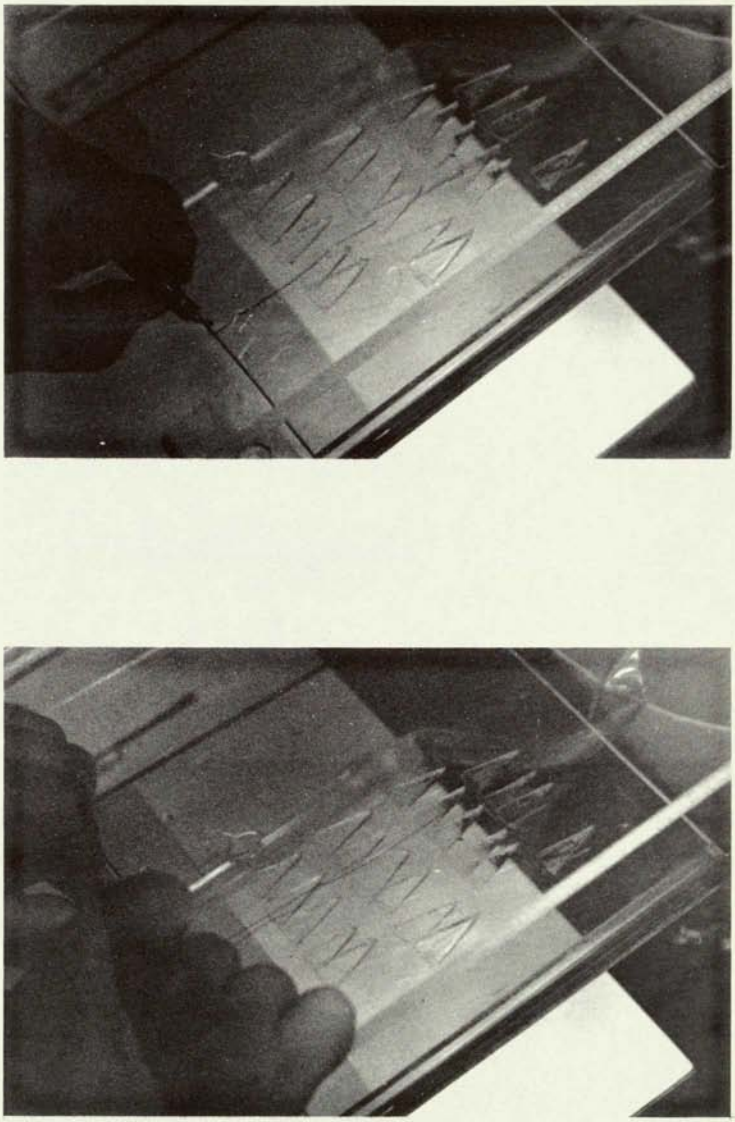

Figure II-16. Photos of Dyed Stream Lines in the Small Test Apparatus (Note Cross-Over of Stream Lines)

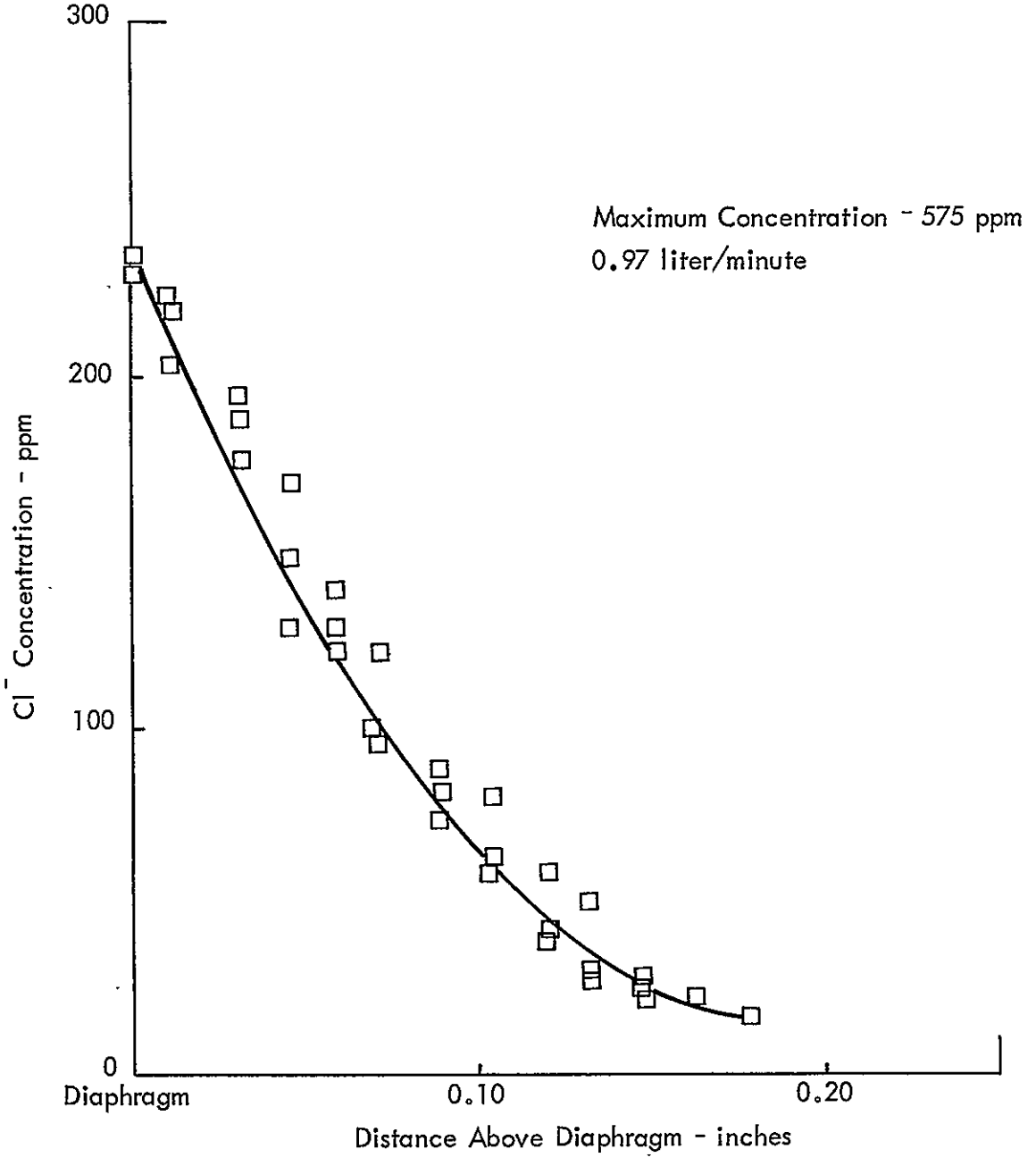

Figure II-17. A Typical Concentration Profile in an Unperturbed Channel

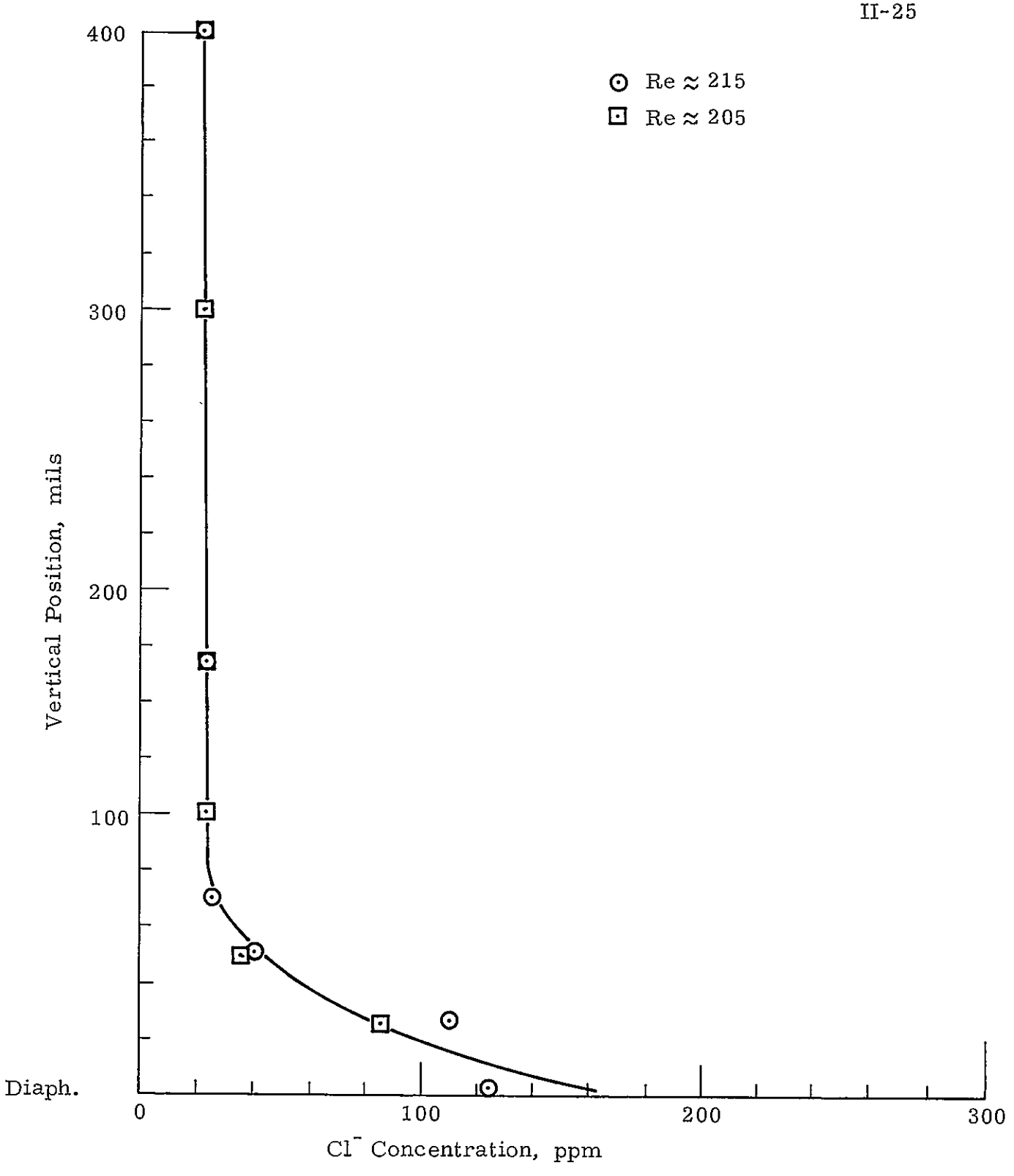

Figure II-18. Concentration Profiles for Various Reynolds Numbers in Straight Channels

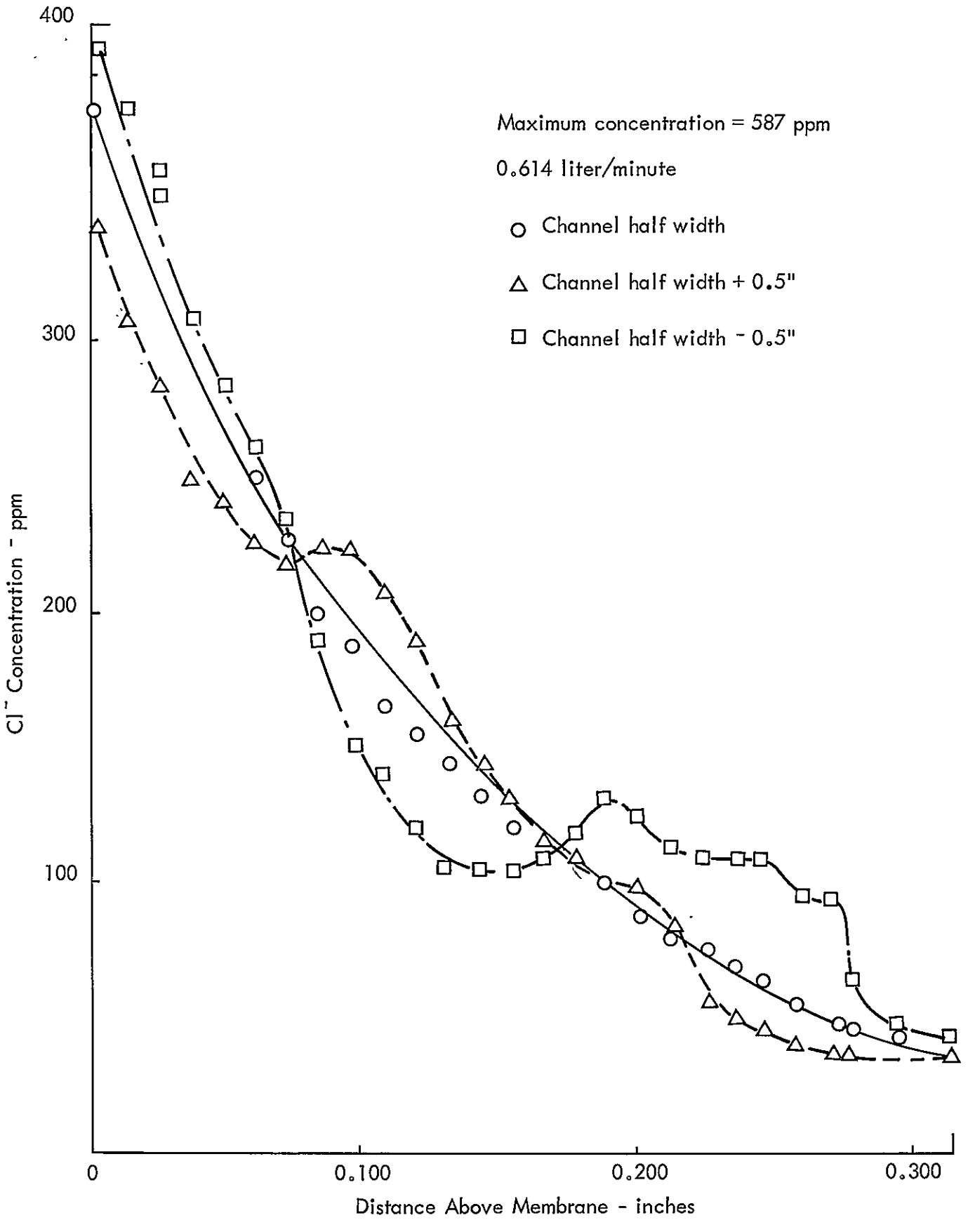

Figure II-19. Concentration Profile in a Test Channel With Secondary Flow

Reynolds number as that shown in Figure II-17. The effects of the vortices in creating secondary flow meanders are clearly evident.

III. RESULTS AND DISCUSSION

A. Summary of Experimental Data

A schematic representation of the scaled-up model test apparatus is shown in Figure III-1. Tap water flowed by gravity into a diverging-converging inlet plenum through the upper dialyzer channel to the drain. The elevation head was established by an overflow pipe and a recycle pump. The 600 parts per million (ppm) salt solution in the lower channel was handled by identical hardware except it was returned to the lower recycle supply tank.

Concentration profiles were obtained by traversing the platinum wire conductivity probe. A Tektronics 25 KHz carrier amplifier and a 561 oscilloscope were used for probe readout. All concentration profiles were obtained in the dilute channel for instrumentation convenience.

A normalized plot of the concentration profiles obtained for the base-line, unperturbed flow case is given in Figure III-2. The data were taken in the dilute channel and extrapolated into the membrane and concentrated channel regions. The purpose of this family of curves is to show relative effects and trends in a single graph. On the right side of the graph are the concentration profiles measured in the dilute channel for various flow rates as indicated. These curves are normalized in Cl^- concentration to the values of concentration existing in the lower (concentrated) channel at the beginning of each run. They are normalized in position to the maximum channel height (0.310 inch). The complete curve for Q = 2.8 liters per minute was constructed by assuming that the concentration profile in the concentrated channel had the same shape as the profile in the dilute channel since the flow rate was the same in both channels. This assumption permits construction of the Q = 2.8 liters per minute curve on the left side (concentrated channel) of Figure III-1. Then, using a straight line approximation to the concentration profile at Q = 2.8 liters per minute, the width of the central region of the graph is determined. This central region corresponds to an additional thickness of liquid film in the concentrated channel which is equivalent to the membrane resistance to mass transfer. Once this equivalent film thickness has been determined, the slopes of the other two curves (Q = 1.04 and Q = 0.56 liters per minute) in this central region of the graph can be calculated based on the total mass transfer rates measured for these runs. Finally, the continuation of these two curves into the concentrated channel portion of the graph were made by drawing a smooth curve from the C/C_{max} level to the intercept of each curve with the line separating the concentrated channel region from the equivalent film thickness region. These smooth curves are drawn to be similar in shape to the curve drawn for the Q = 2.8 liters per minute case. The trends in the results are clearly shown by this family of curves. The difference in slope through the equivalent film resistance and concentrated channel boundary layer is indicative of the difference in the mass transfer rate for the various flow rates tested. As flow rate decreases, the rate of mass transferred (flux) decreases

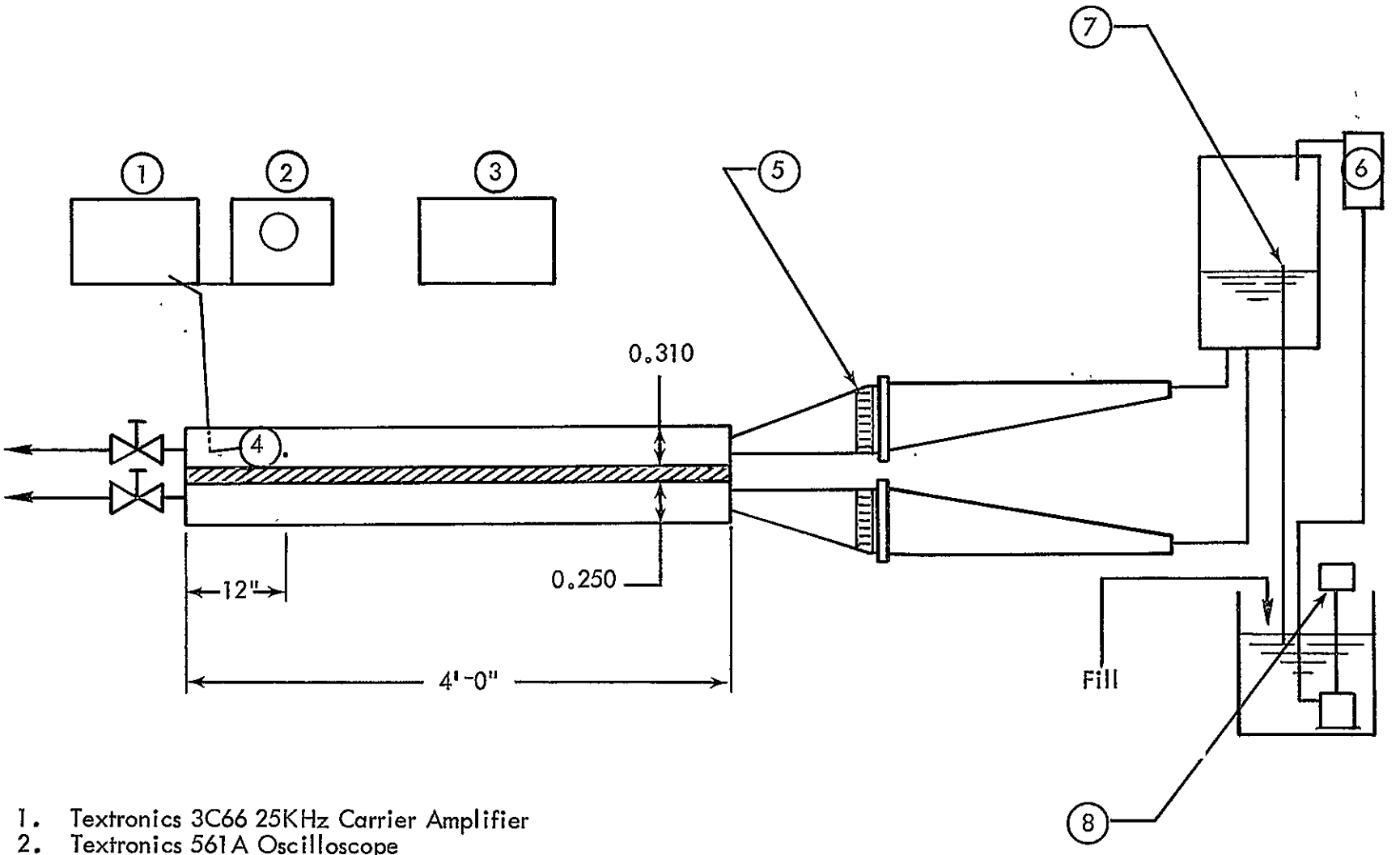

1. Textronics 3C66 25KHz Carrier Amplifier
2. Textronics 561A Oscilloscope
3. Bubble Generator
4. Concentration Probe
5. Flow Straightener
6. Filter
7. Overflow Pipe
8. Recycle Pump

Figure III-1. Schematic Representation of the Test Apparatus

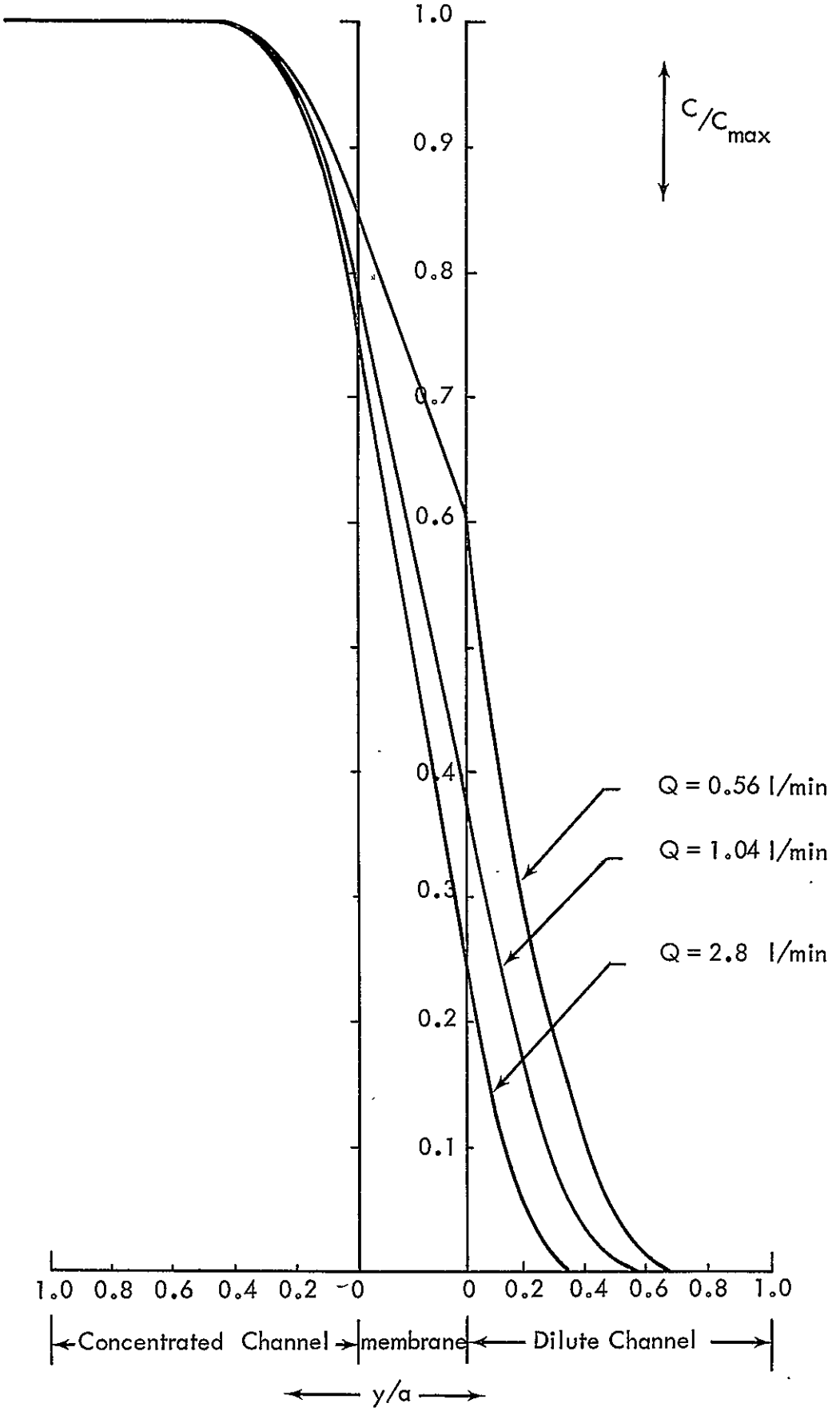

Figure III-2. Normalized Concentration Profiles for the Unperturbed Cases

even though the average concentration (area under the concentration versus height curve) increases. This decrease in flux is readily seen in Figure III-1 as a decrease in concentration gradient through the equivalent film resistance with decreasing flow rate.

A similar normalized plot is given in Figure III-3 for the perturbed case in which membrane supports of the type shown above in Figure II-15 were used. This plot was generated in the same way as the curves in Figure III-2. The curves on the right side of the plot, in the dilute channel, were derived from measured data. The remainder of the plot was generated using the same type of extrapolation just described.

During each run with both the unperturbed and perturbed flow patterns, a measurement was made of the steady-state mass transfer rate. Figure III-4 shows the results of these measurements of mass transfer rate as a function of flow rate.

B. Interpretation and Discussion

1. Theoretical Considerations

It has been shown by Babb that mass transfer in any parallel plate dialyzer in which fully developed two-dimensional laminar flow exists is determined by the dimensionless group Pa/D, the wall Sherwood number (Ref. 7). In this expression "P" is the membrane permeability to a specific solute, "a" is half the spacing between the parallel plates, and "D" is the diffusivity of the solute in the particular solvent. Babb further states that the curve shown in Figure III-5 will give the relation of the overall mass transfer coefficient to the wall Sherwood number and that the blood channel height may be optimized by the relation shown in Equation (1) given in the figure. This relation does not include the consideration of secondary flow.

The curves in Figure III-5 show that as wall Sherwood number increases, the liquid film resistance becomes an increasing portion of the total resistance. For maximum dialyzer efficiency it is desirable for the membrane resistance to equal the overall mass transfer resistance. This implies that from an efficiency standpoint one should attempt to minimize Sherwood number. Since we always want membrane permeability to be as high as possible, Sherwood number may be minimized only by decreasing the half channel height or by increasing diffusivity.

There is a tendency to assume that diffusivity is not a variable once a given diffusing specie and solvent are defined. If one makes that assumption then the Sherwood number may be decreased only by decreasing channel half height. While it is true that absolute diffusivity is fixed by the diffusing specie and the solvent system, it is possible to increase the effective diffusivity by mixing. Hittman Associates approached the problem of reducing Sherwood number by attempting to increase the effective solute diffusivity. The curves in Figure III-6 are helpful in visualizing what is occurring in a typical channel with parallel laminar flow.

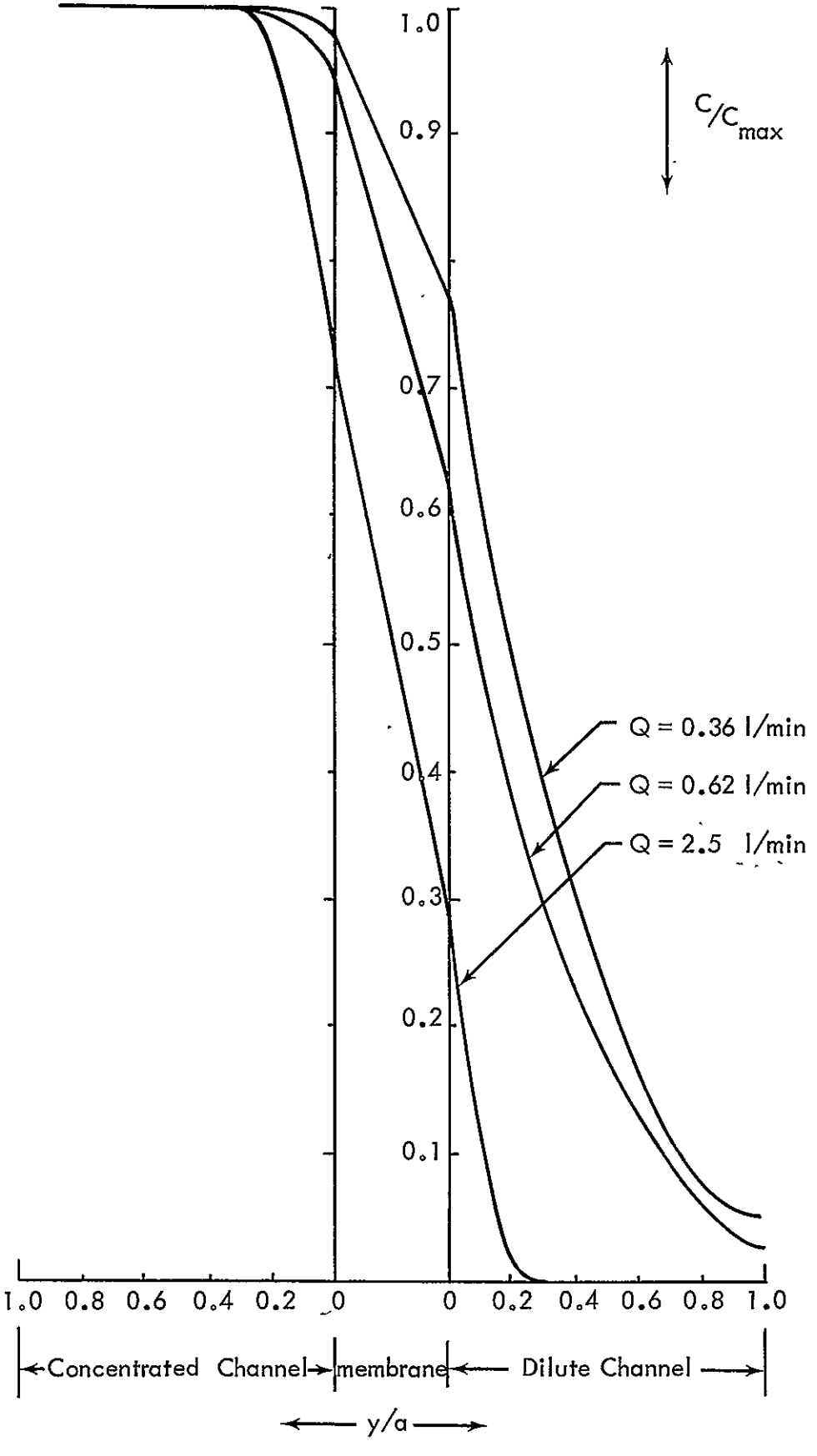

Figure III-3. Normalized Concentration Profiles for the Perturbed Case

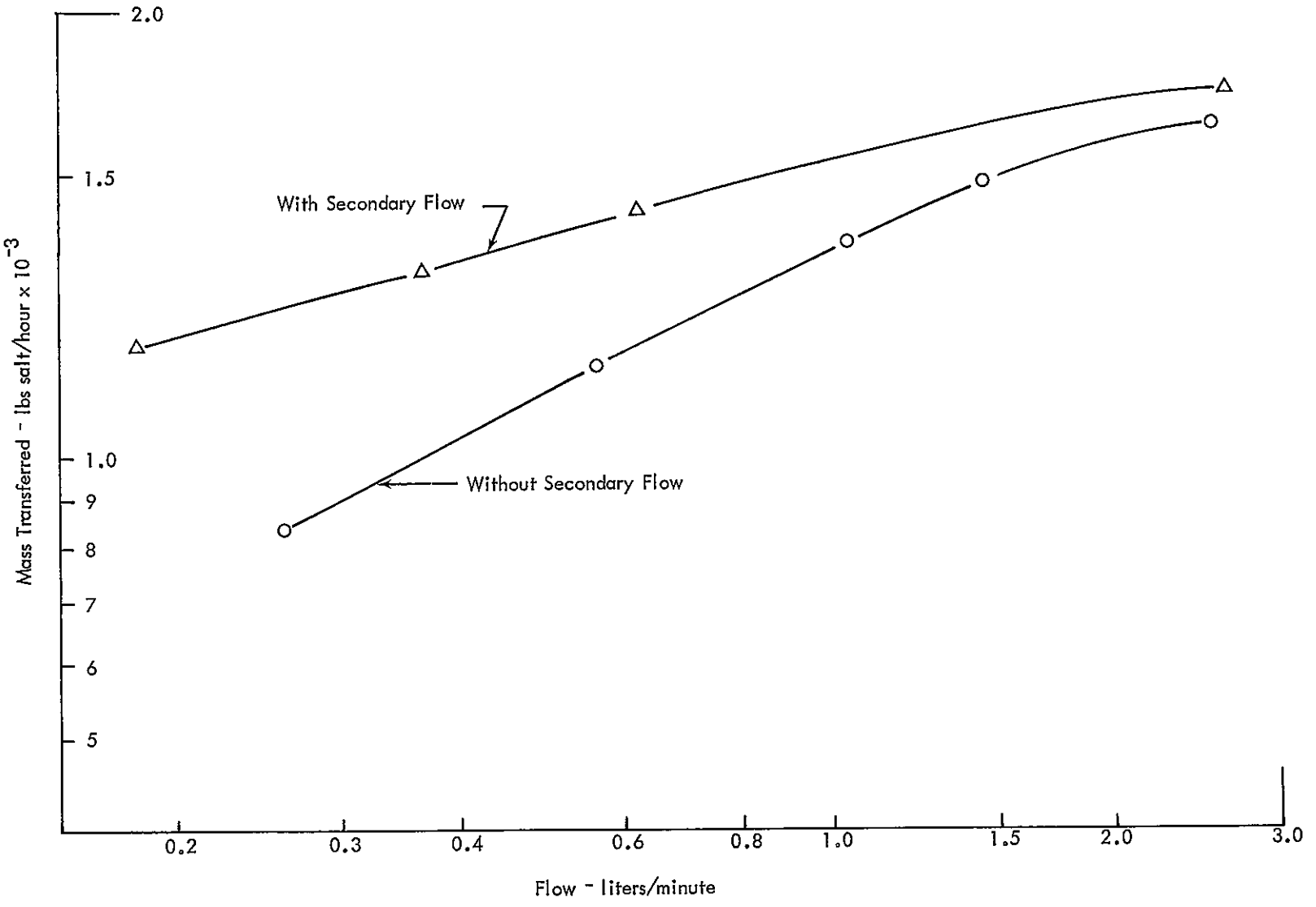

Figure III-4. Effect of Secondary Flow on Improving Overall Mass Transfer Rate

$$a_{opt} = 1.6\sqrt[3]{\frac{h_o \mu l^2}{\Delta P}} \qquad (1)$$

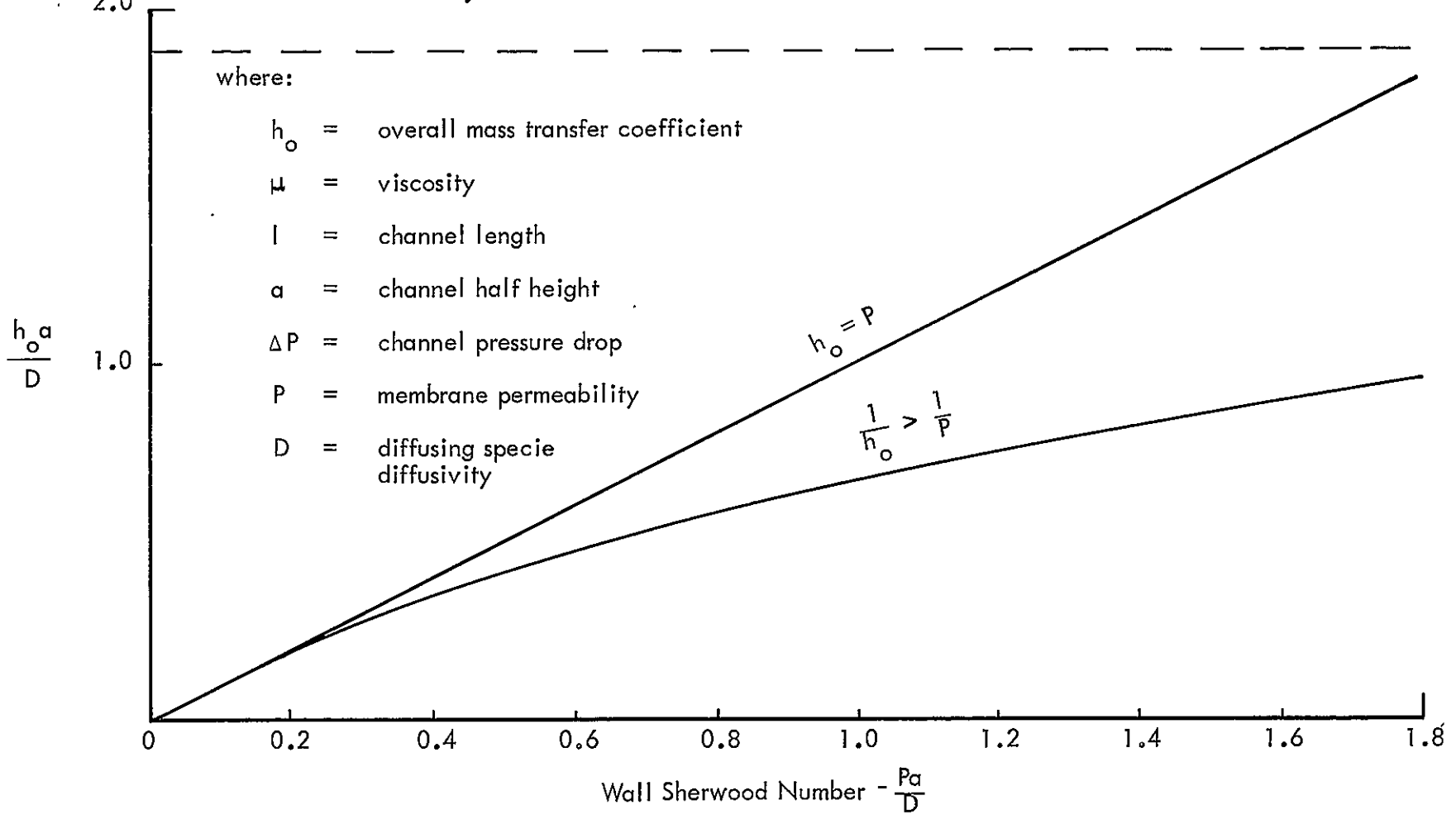

Figure III-5. The Increasing Effect of the Blood Film Resistance as the Wall Sherwood Number Increases

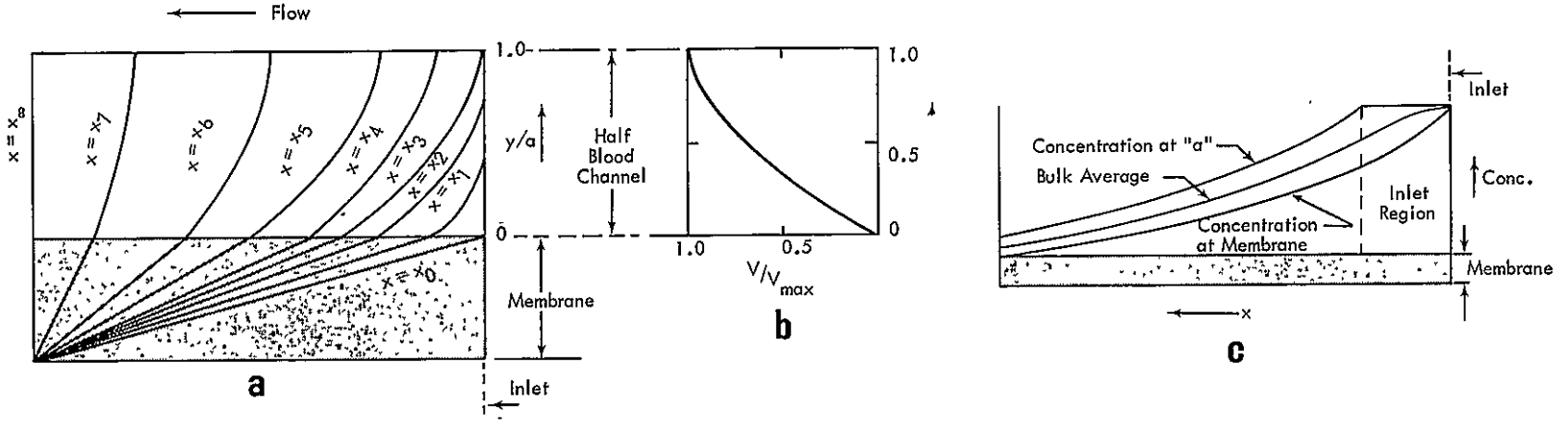

Figure III-6. Normalized Two-Dimensional Flow and Concentration Profiles Between Semi-Infinite Permeable Parallel Plates

In constructing the concentration versus thickness curves (III-6a), zero film resistance and zero concentration change were assumed on the dialyzer channel side of the membrane and the inlet fluid was assumed to be in fully developed parallel laminar flow as indicated by the velocity profile in (III-6b). The curves, $x = x_o$, x_1, etc. indicate the concentration profiles at increasing distances down the channel. It was further assumed that the channel is symmetrical about the half channel plane. The symmetry assumption requires that the slope of the concentration versus position curves be infinite at the half channel plane and the slope of this curve at the membrane is a function of the ratio P/D. For fixed membrane conditions the slope of the gradient within the membrane uniquely defines the mass flux through the membrane and hence the rate of depletion of the blood half channel.

There is a finite time, hence a finite distance down the channel, before the concentration at the half channel position begins to change. This distance over which the concentration boundary layer develops defines the "inlet region." Within this region the concentration gradient across the channel increases from zero at the inlet to a maximum value which it attains at the end of the so-called inlet region. As fluid passes down the channel beyond the inlet region the difference between the membrane concentration and the average concentration decreases as is shown in Figure III-6c. There are two points of interest here. Regardless of location along the channel the membrane concentration is always less than the average concentration. Further, a close approach of the membrane concentration to the average concentration can only be obtained in parallel flow by allowing the mass transfer through the membrane to decrease. In systems without secondary flow where the mass flux is allowed to decrease to the point that the concentration at the membrane approaches the average concentration, the terminal difference is very small and the membrane area is not being utilized effectively.

If we could mix the fluid above each x location to its average concentration, the mass flux through the membrane would increase proportionately to the increase in concentration gradient across the membrane. If we were not restricted by maximum allowable blood velocities we could use turbulent flow to provide the required mixing action. Fortunately, the mixing effects of turbulence may be obtained at low Reynolds numbers by inducing secondary flow. The eddy diffusion which results from this secondary flow effectively increases the solute diffusivity and decreases the wall Sherwood number.

As we have seen, if we can reduce wall Sherwood number without decreasing membrane permeability we achieve our objective of improving the dialyzer overall mass transfer rate.

In our experimental program to investigate the effectiveness of various techniques of introducing secondary flow, the physical size requirements of the instrumentation necessary to measure the velocity and concentration profiles made it mandatory that the simulated blood channel be scaled upward. The test channel was increased to a nominal 0.310 inch height and a 10 inch width. If the channel scaling were held in length, the

device would have to be over one hundred feet long. For practicality, we chose to operate only in the inlet region. The length of this region was calculated to be somewhat in excess of four feet for lowest flow unperturbed case. Since mixing will shorten the inlet region length, we set the test apparatus length at four feet. The concentration difference across the blood channel varies from zero at the channel inlet to a maximum at the end of the inlet region and decreases thereafter. In the limit, it will reach zero in an infinitely long channel. By operating only in the inlet region conservative approximation is made of the improvement which secondary flow will bring about. This is true because the area weighted gradient across the channel of the test apparatus is less than the area weighted gradient in a length optimized operational device.

2. Interpretation of Data

Referring to the results obtained for the baseline, unperturbed case, shown in Figure III-2, it can be seen that as the total flow decreased concentration at the membrane increased and the flux through the membrane is decreased. These data show that we were clearly in the inlet region and that our initial predictions of the length of this region were approximately correct.

It must be remembered that we were measuring in the dilute channel for instrumentation convenience and that the blood channel case would be a mirror image of that shown here.

Referring to the results obtained for the perturbed flow case shown in Figure III-3, it can be seen that the effective length of the inlet region has been reduced by the introduction of the vortex generators, since the data clearly show that the centerline concentration has now been decreased within the same experimental channel length. Part of this change was due to the decreased average channel height caused by the lands of the vortex generators. This change was not sufficiently great to account for the decrease in observed inlet region length.

Since the length of the inlet region has decreased, and this length may be shown to be a function of wall Sherwood number, we must conclude that wall Sherwood number has decreased. We have shown that Sherwood number may be decreased only by decreasing the average half channel height or increasing the effective solute diffusivity. Since the known change in half channel height cannot account for the observed change in the inlet region length, we must conclude that eddy diffusion has increased the effective solute diffusivity.

Figure III-4 shows the change in observed overall mass transfer with changes in flow for the baseline and perturbed cases. The unperturbed case, without secondary flow, is linear up to a flow of 1.2 liters per minute; above this value the membrane is obviously controlling mass transfer. Over the linear portion of the curve the slope equals 0.5. This is what would be expected for fully developed laminar flow between parallel plates in the mass transfer inlet region where the thickness of the depleted zone (or

enriched zone in this experiment) is primarily a function of the fluid boundary layer thickness.

For the perturbed flow case, an improvement of 50 percent was obtained at the low flow rates for which Reynolds numbers were comparable to those in actual hemodialyzers. This improvement was obtained with membrane supports of the type shown in Figure II-15 and could be easily introduced into the design of an otherwise conventional Kiil dialyzer.

The effect of the vortex generators is to decrease the mass transfer dependence on flow rate which is as expected. These data show that it is possible to increase the relative performance of a dialyzer by control of the blood side velocity profile. Since the tests discussed here were conducted in the so-called concentration boundary layer inlet region, they will overpredict the absolute mass transfer in a practical scale dialyzer. However, by operating only in the inlet region we have made a conservative approximation of the relative improvement which secondary flow will bring about. This is the region in which it is most difficult to cause a relative increase in mass transfer since, as can be seen in Figure III-6c, the concentration driving force at the membrane is high even for the laminar, unperturbed case.

The data developed in this experimental program show that secondary flow can be a powerful tool in improving overall dialyzer mass transfer rate.

REFERENCES

1. Clutter, D. W. and A. M. O. Smith, "Flow Visualization by Electrolysis of Water," Aerospace Engineering, 20, January 1961, pp. 24-7, 74-6.

2. Kovasznay, L. S. G., private communication.

3. Smith, K. A., C. K. Colton, E. W. Merrill, and L. B. Evans, "Convective Transport in a Batch Dialyzer: Determination of True Membrane Permeability from a Single Measurement," The Artificial Kidney, Chemical Engineering Progress Symposium Series No. 84, Volume 64, 1968.

4. Meltzer, T. H., K. Gutfreund, V. K. Kulshrestha, and A. M. Stake, "Optimized Cellulose Membranes for Artificial Kidney Dialysis Applications," Transactions of the American Society for Artificial Internal Organs, 14, 1968, pp. 12-8.

5. Bluemle, L. W., Jr., Proceedings from the Conference on Hemodialysis, National Institutes of Health, 1964, pp. 96-8.

6. Lande, A. J., B. Parker, V. Subramanian, R. G. Carlson, and C. W. Lillehei, "Methods for Increasing the Efficiency of a New Dialyzer-Membrane Oxygenator," Transactions of the American Society for Artificial Internal Organs, 14, 1968, pp. 227-30.

7. Babb, A. L., "Fluid Mechanics, Mass Transfer, and Optimization Studies of Hemodialyzers," First Summary Report, Contract No. PH-43-66-932, University of Washington, Seattle, November 1, 1967.

APPENDIX A. DESIGN DETAILS OF THE SCALED-UP MODEL

The main test frame assembly is shown schematically in Figure A-1. The design utilizes a highly effective method of obtaining uniform laminar flow. Co-current flow of the test solution (water) occurs in the top section, with a concentrated saline in the lower section. Co-current flow is used to maintain a uniform pressure difference across the membrane. The entrance plenums are designed to fully expand and develop laminar flow and allow full flow development near the entrance of the test section. Detailed drawings of the plenums are shown in Figure A-2, a, b.

The unit was assembled in a wooden test frame constructed as shown in Figure A-3. The short plenum section was mounted permanently with two pins (one-eighth inch), three-quarter inch by one-quarter-20 stainless steel screws, and PC-7 epoxy adhesive to prevent leakage problems. A slight five degree angle was milled on the feed end of the test holder frames (Figure A-4) to allow sufficient clearance between the plenums. Extra-large "O" ring stock was used for a better seal to the plenum and between the test frame pieces (0.139 inch diameter "O" ring stock - BUNA-N).

The plastic flow channel inserts, as shown in Figure A-5, were permanently mounted in the aluminum test section. The original design called for an "O" ring mounted in a "V" channel between the edge of the metal test frame holder and the plastic insert; however, due to cumulative tolerance problems, the "O" ring seal was unsatisfactory.

A metal frame, fabricated from one-half inch by one-half inch aluminum bar stock, was made and holes drilled to match those in the plastic insert. Since a gasket of finite thickness would change the inner tolerances in the test section, a thin film of RTV silicone rubber (General Electric) was applied to the frame. When the insert was bolted tight with the hold-down frame, a very thin film of RTV was left which cured in place. This method of sealing proves to be quite satisfactory.

The slight gap between the metal test frame and the plastic insert was filled with acrylic molding compound (Klearmount) which was allowed to harden. Since the tolerances on Plexiglas sheet are poor, it was necessary to taper the inside surface of the plastic to be even with the metal frame. Dental-type grinding and polishing tools were used for this operation.

The assembled unit was placed on the wooden frame. Piping connections were made using three-quarter inch copper tubing with three-quarter inch Swagelock (ZY-1210-1-12) fittings for connections to the test frame. Other connections were made with copper soldered tubing connections.

The supply reservoirs were nominal 53 gallon polyethylene tanks (McMaster-Carr 4330-K-2). It is necessary to throttle back the flow from the sump pumps so that the flow through the stand pipe overflow is just greater than the recirculating volume from the pump.

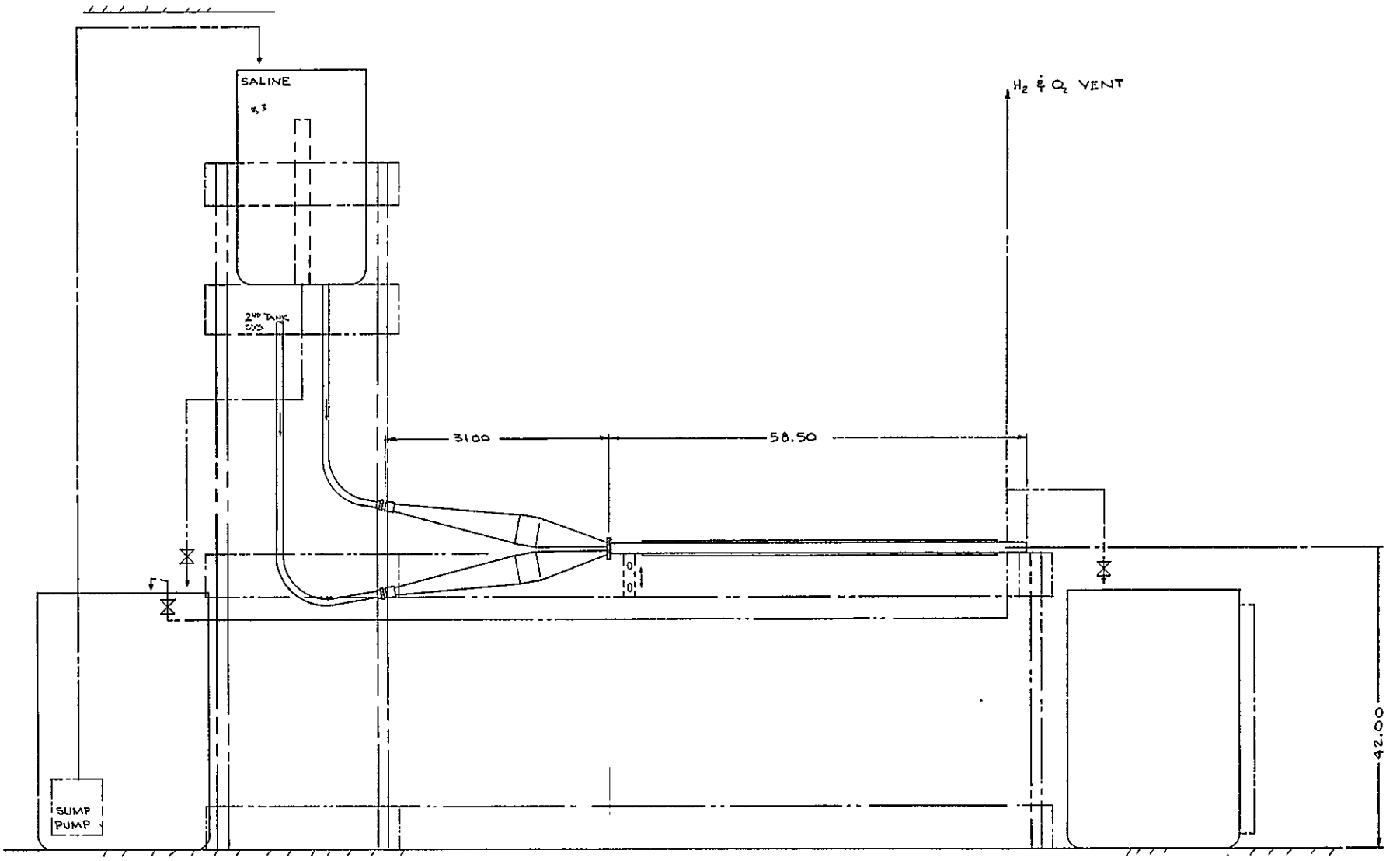

Figure A-1. Layout of Scaled-Up Model

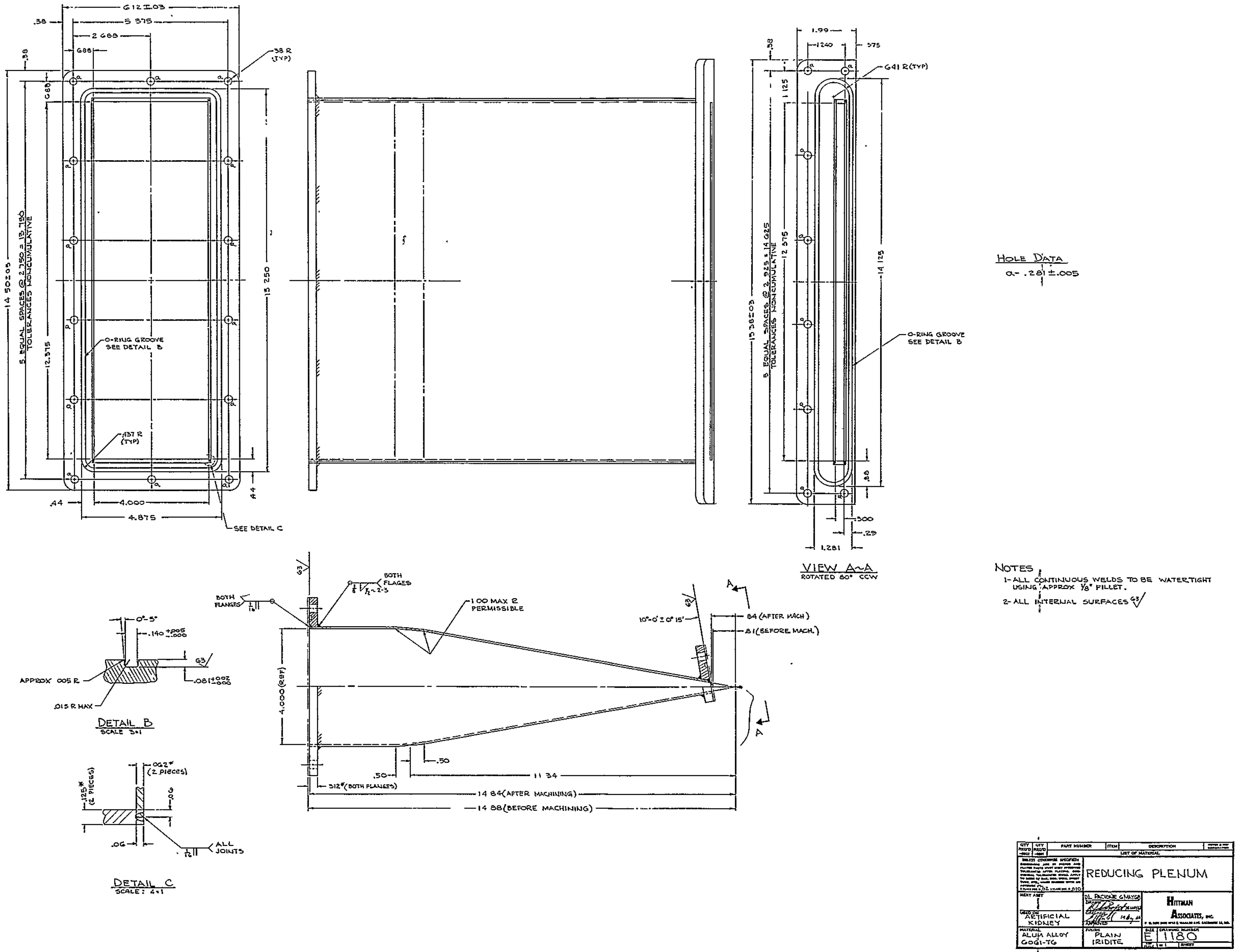

Figure A-2a. Detailed Working Drawing Plenum Section

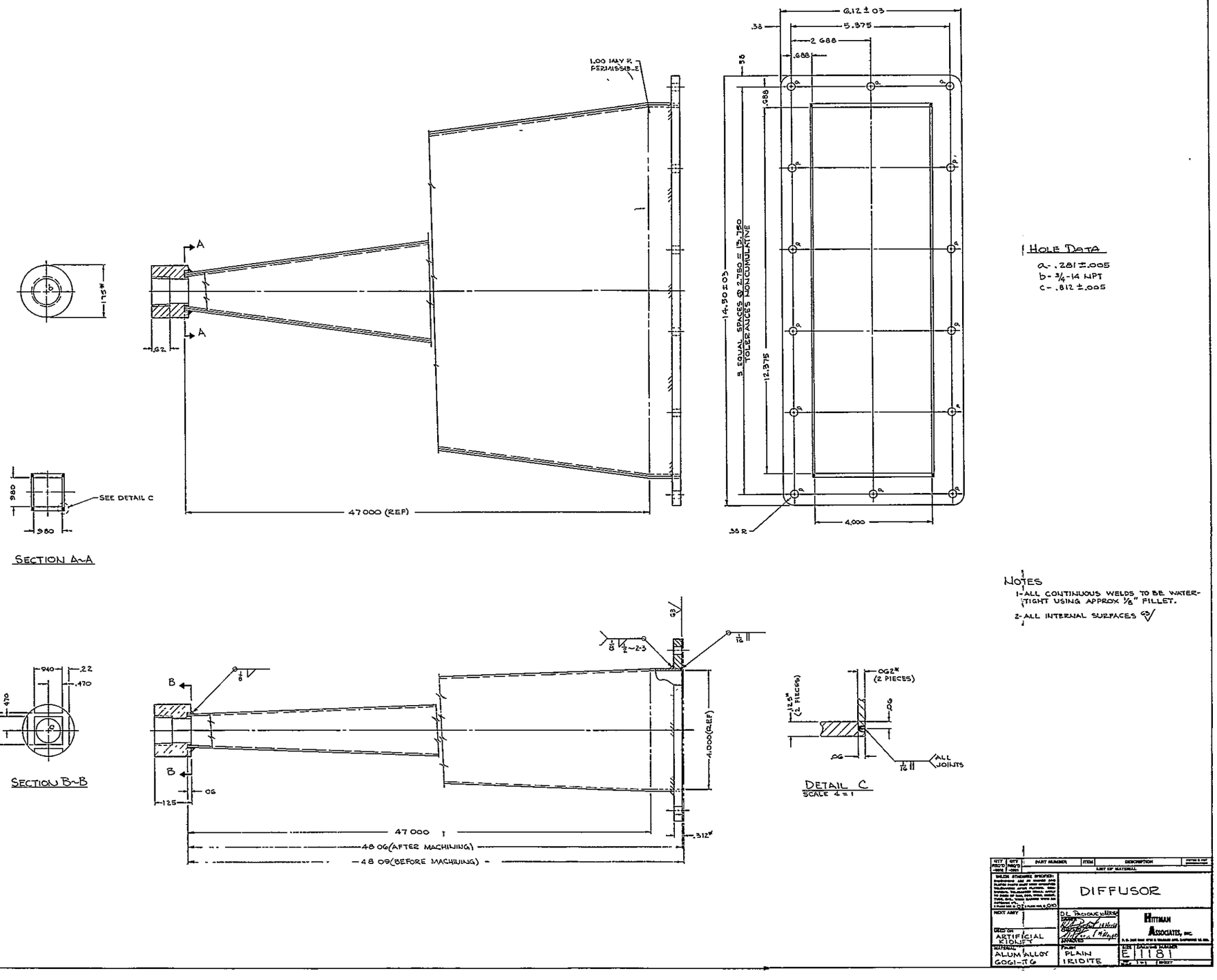

A

B

Figure A-2b. Detailed Working Drawing Plenum Section

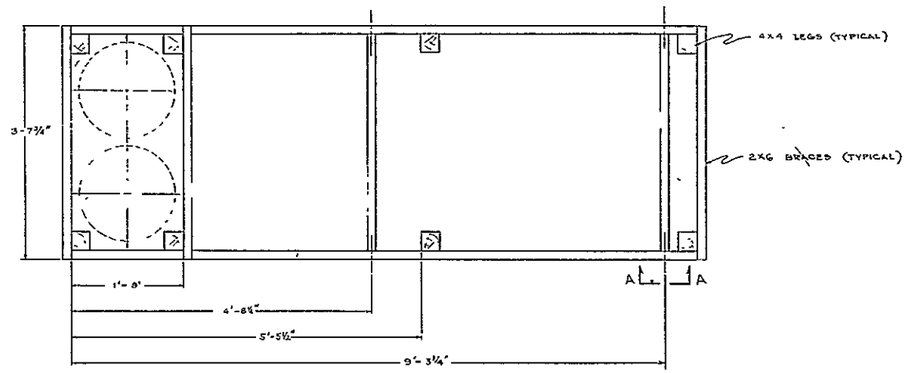

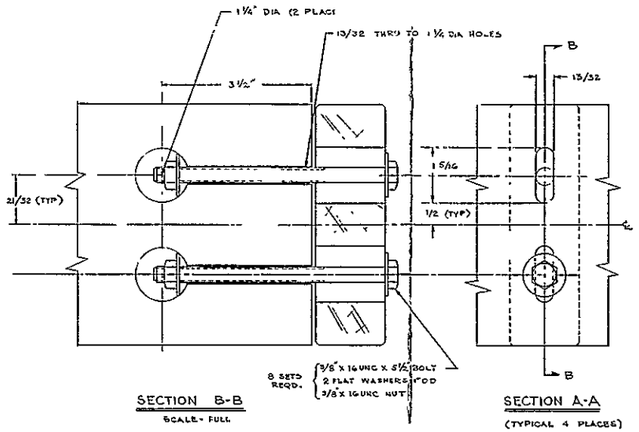

SECTION B-B
SCALE- FULL

SECTION A-A
(TYPICAL 4 PLACES)
SCALE - FULL

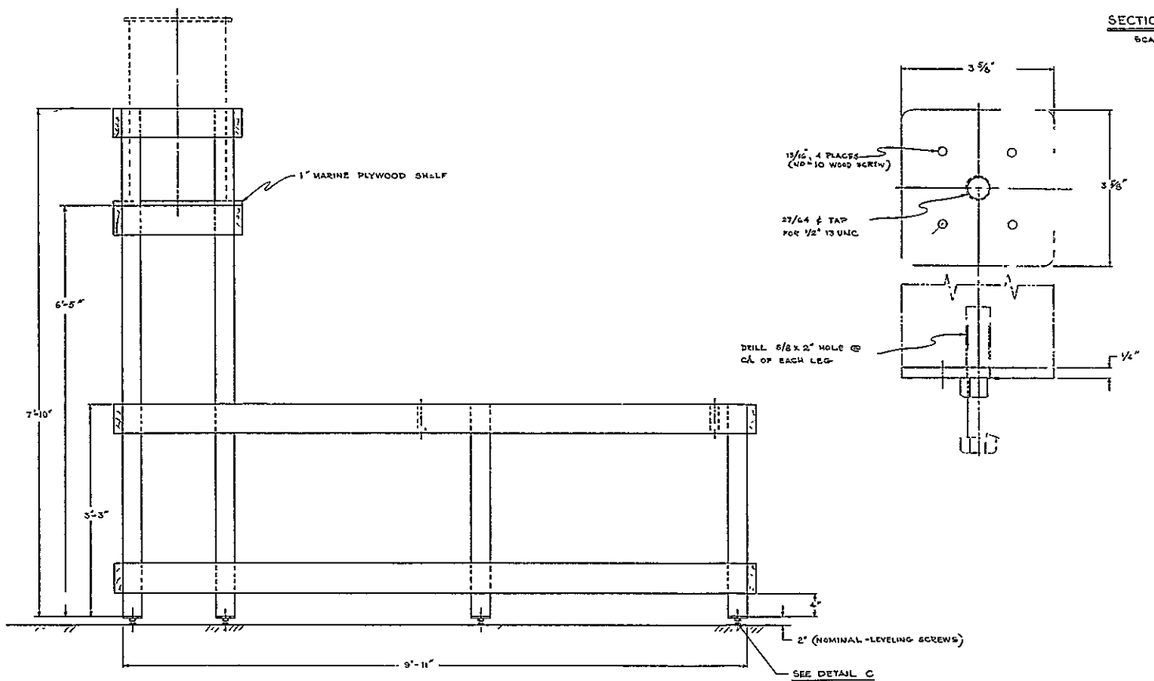

6 PIECES 4"x4"x8'
6 PIECES 2"x6"x8'
4 PIECES 2"x6"x10'
PIECE 1"x 2"x 4' MARINE OR EXTERIOR)
LBS #10 COMMON

B

A

Figure A-3. Detailed Construction of Stand for Model Unit

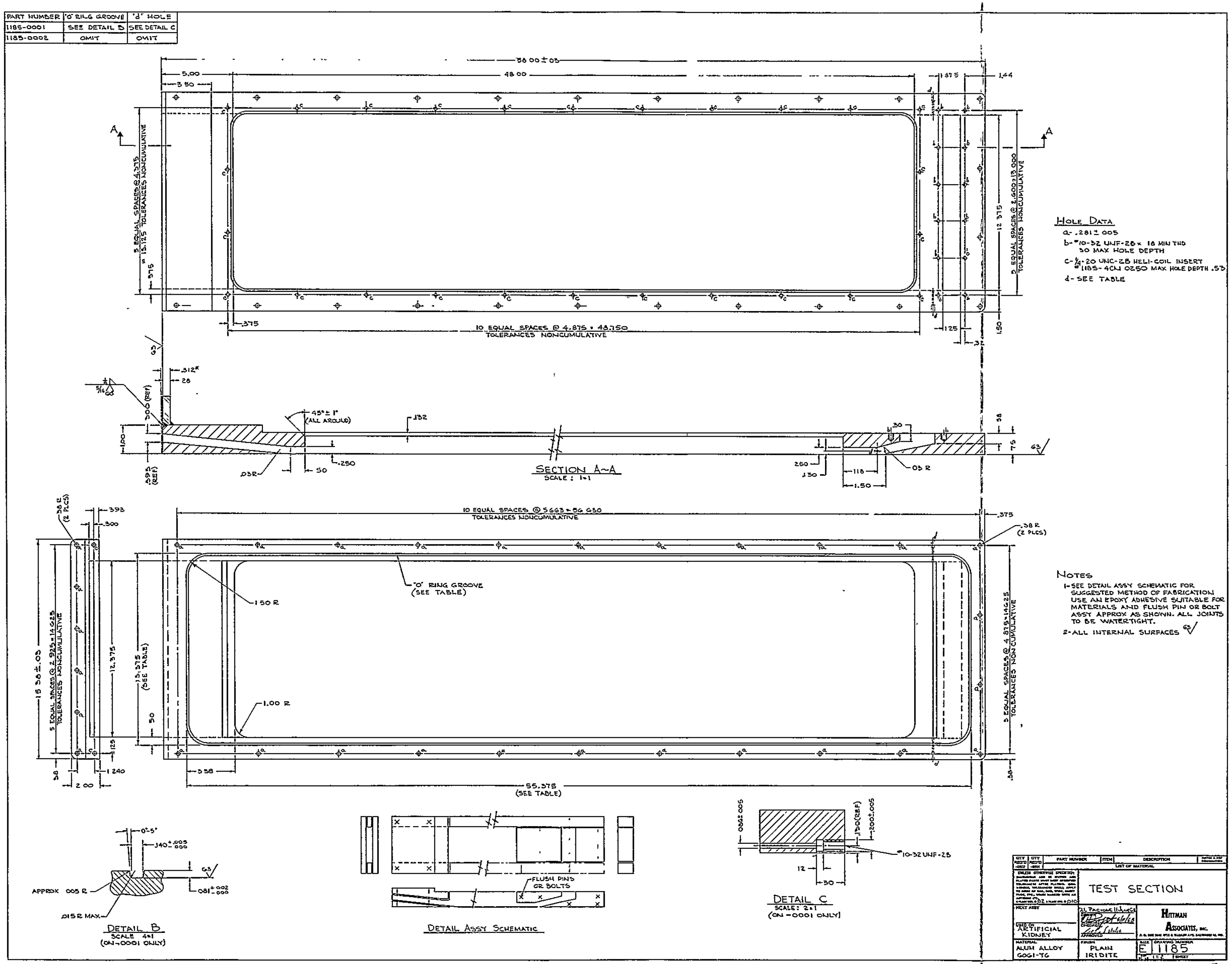

Figure A-4. Aluminum Test Section Frame

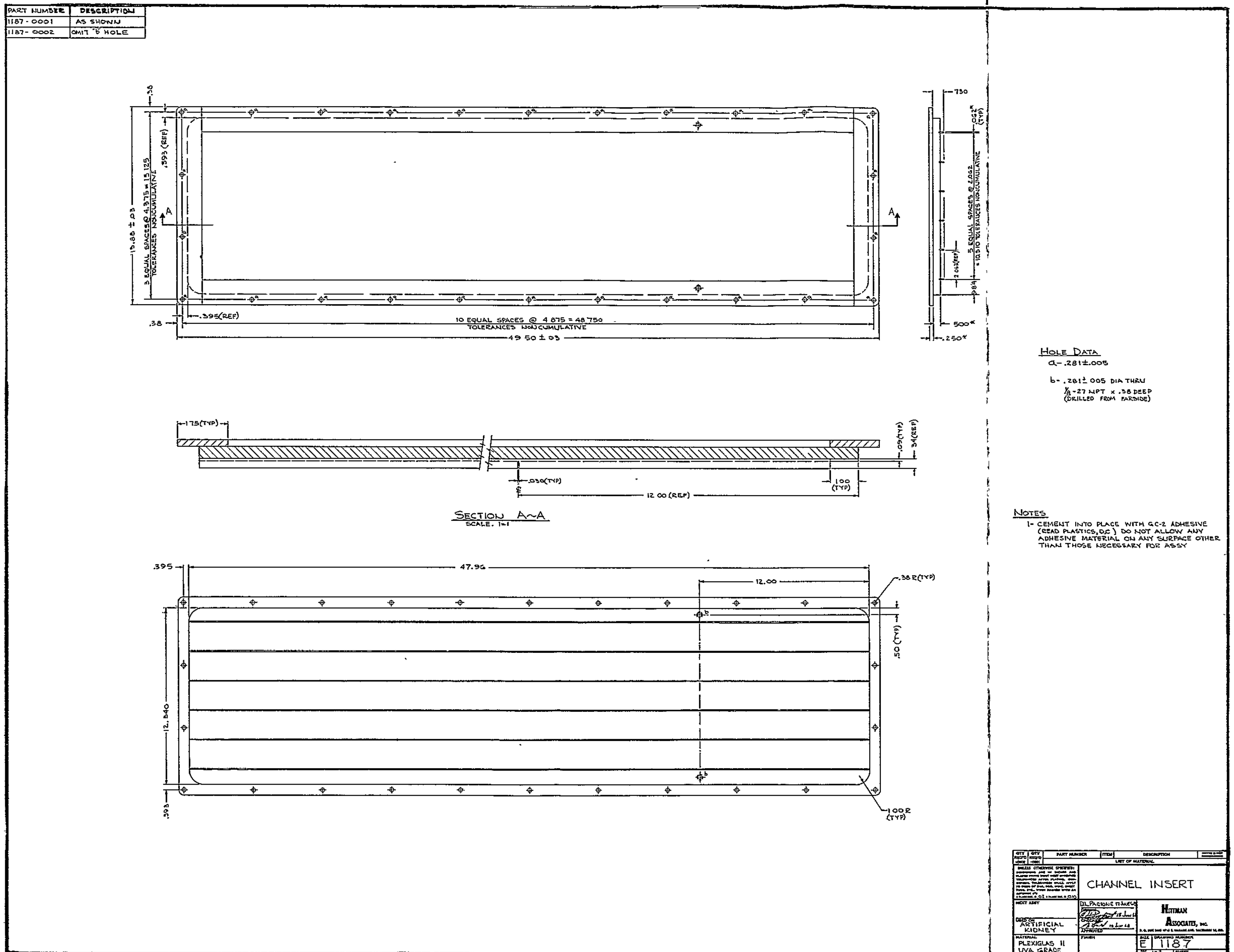

Figure A-5. Plastic Channel Insert with No Perturbations

A section of hexagonal aluminum honeycomb one inch thick with 0.15 inch by 0.10 inch openings was inserted in the large section of the plenums to provide additional flow straightening.

Two rubber serum vial caps were mounted in two channels (channels 2 and 4) at the feed end of the plastic insert. The opening under the caps was filled with cured RTV rubber trimmed to be level with the upper surface of the insert so that no flow perturbations are introduced. Dye could be injected into the channels to check flow patterns using an 18 gage, one inch hypodermic needle and a Harvard infusion pump.

In addition, two pressure taps at the upstream and downstream ends of the upper flow channel were made by drilling one-quarter inch NPT holes and using one-quarter inch Swagelock male connectors.

Various methods were tried to insert the cellophane under mild tension so that it would not sag between the channels. The only method that worked was to pre-wet the cellophane in a photographic tray for 10 minutes before hand stretching over the lower test frame. Originally, the two halves of the test frame were held together by bolts pressing on the 0.139 inch "O" ring but tears propagated from the bolt holes. Therefore, the test sections were held together by eight-inch deep-throat "C" clamps (Williams No. 408).

For assembly, the "O" ring was cleaned and coated lightly with silicone vacuum grease. The cellophane was soaked as above and stretched over the lower test frame. The top test section was placed over the wet cellophane as rapidly as possible since rapid drying of cellophane (and subsequent shrinking) could occur. The clamps were tightened in alternating sequence, pulling the cellophane carefully taut before each clamp was fastened. If care was exercised, rippling of the cellophane could be avoided.

After the unit was assembled, all of the air was carefully bled out of the test sections by alternately opening and closing the upper and lower exit valves.

A fine cloudy floculant contaminant was found originally in the test unit, presumably a waxy mold release agent breaking free of the polyethylene storage tanks. To combat this, a Cuno six gallon per minute, five micron cartridge water filter (Model P10-1) was installed in each recirculating pump outflow line.

Also, to obtain more accurate flow control, one-quarter inch orifice plates were installed in both the upper and lower exit lines, just before the exit valves.

With a 24 inch head in the feed tank, flow through the upper channel was approximately 2.2 gallons per minute at maximum flow. This gave a Reynolds number in the test section of about 452. This was the maximum possible Reynolds number with this equipment. Most test data was taken over the range of Reynolds numbers from 5 to 100.

APPENDIX B. MEASUREMENT OF CONCENTRATION BY MEANS OF A CONDUCTIVITY PROBE

Concentration of ions in solution can readily be determined by measurement of the electrical conductivity of the solution. Measurement of conductivity at a point in a scaled-up model dialyzer channel involves a few complications not usually encountered when static measurements are made in a "conductivity cell." It is expected that, in the dialyzer channel, there will be a gradient decreasing away from the membrane in the concentration of ions. Since the dimensions of any conductivity probe cannot be infinitesimal, the probe will necessarily measure an average conductivity in the region of the probe. However, because of the nature of the electric field pattern in the neighborhood of the tip of the probe, it is possible to limit the region under observation to a small volume surrounding the tip.

The effect of probe dimensions on the size of the observed region can be obtained by examining the mathematical formulation of the resistance between two concentric spheres as shown in Figure B-1. In this case, for simplicity, it will be assumed that the conductivity of the

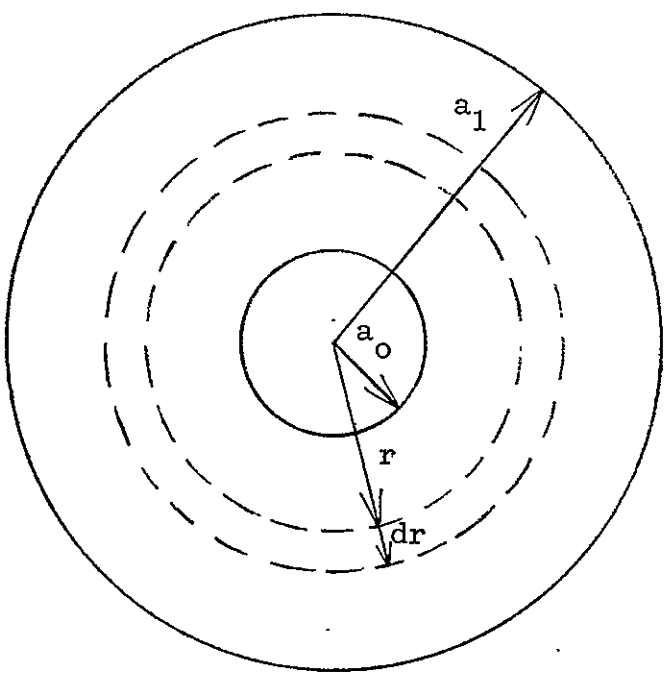

Figure B-1. Idealized Configuration of a Conductivity Probe

medium between the spheres varies only with radius. The resistance of each spherical shell of thickness dr is added to that of all the others, i.e.,

$$R = \int_{a_o}^{a_1} \frac{\rho(r)}{4\pi r^2} \, dr \qquad \text{(B-1)}$$

where:

R = electrical resistance between spheres at a_o and a_1

ρ = electrical resistivity of the medium, $\rho = \frac{1}{\sigma}$

σ = electrical conductivity

r = radius of spherical shell

dr = incremental shell thickness

Carrying out the integration in Equation (B-1) yields:

$$R = \frac{\sigma}{4\pi a_o} \left(1 - \frac{a_o}{a_1}\right) \qquad \text{(B-2)}$$

where ρ is constant throughout the medium. Examination of the form of Equation (B-1) shows that resistivity (or conductivity) is a weighted average over the region between a_o and a_1 (as rewritten in Equation (B-3)):

$$R = \frac{1}{4\pi} \int_{a_o}^{a_1} \frac{1}{r^2} \rho \, dr \qquad \text{(B-3)}$$

Thus, variations in ρ are decreased in effectiveness by the square of the distance from the center of the sphere. For example, when the medium has a uniform resistivity, 80 percent of the total resistance seen between a sphere of radius a_o and an electrode at infinity occurs within a sphere of radius $5a_o$. The graphical relationship is shown in Figure B-2. When the resistivity varies, it is apparent from Equation (B-3) and Figure B-2 that the relative effect of a variation away from the immediate vicinity of the probe is reduced by the square of the distance.

The actual size of the region over which the weighted average of conductivity occurs depends directly on the dimensions of the probe.

If a 0.001 inch diameter probe is used, and if this probe is bare of insulation only within 0.001 inch of its tip, then the conductivity measured by this probe is a weighted average over approximately a 0.010 inch diameter sphere. The "indifferent" electrode is placed some large distance away from the probe. This size is sufficiently small compared to the 0.250 inch channel height to represent a "point" measurement of conductivity.

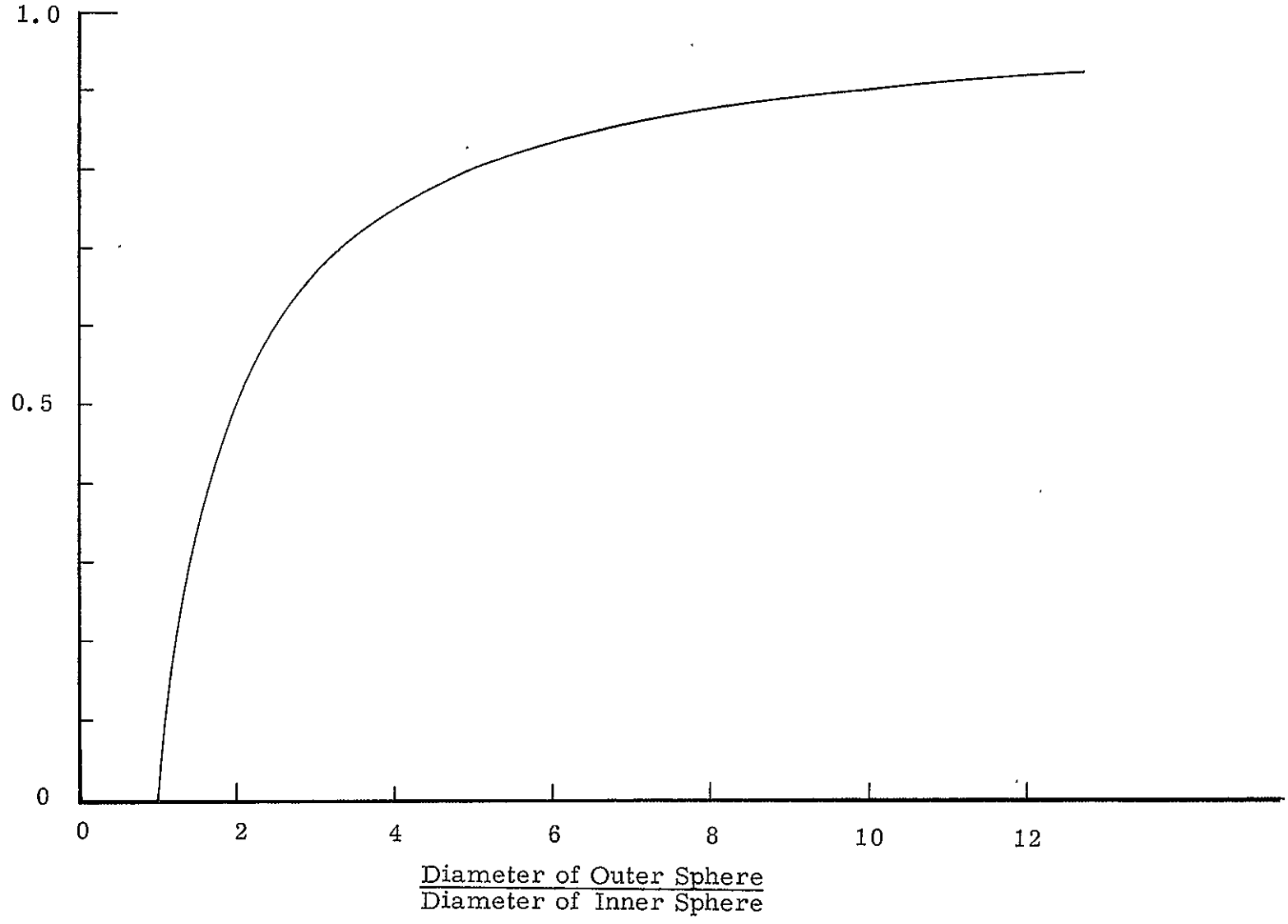

Figure B-2. Region of Observation of a Unipolar Conductivity Probe